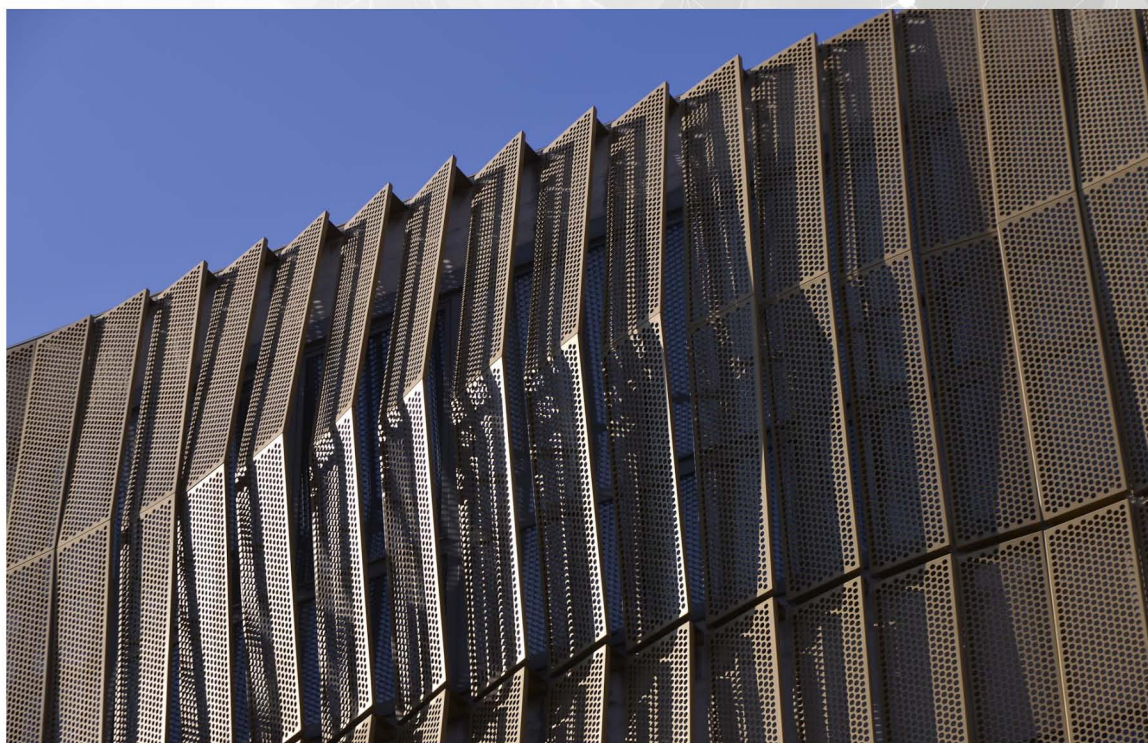


# Book of Extended Abstracts MY FIRST CONFERENCE 2017

## **EDITORS:**

Sandra Kvaternik, Fran Torbarina, Natalija Vitali  
Marko Čanađija, Vanja Travaš, Goran Vukelić



September 28, 2017

Faculty of Engineering, University of Rijeka, Croatia

# **Book of Extended Abstracts – My First Conference 2017.**

## **EDITORS:**

Sandra Kvaternik  
Fran Torbarina  
Natalija Vitali  
Marko Čanađija  
Vanja Travaš  
Goran Vukelić

## **ORGANIZED BY:**

Faculty of Engineering, University of Rijeka  
Faculty of Civil Engineering, University of Rijeka  
Faculty of Maritime Studies, University of Rijeka

ISBN 978-953-6326-92-1

ORGANIZING COMMITTEE:

Sanja Grbac Babić

Sara Grbčić

Mladen Jardas

Sandra Kvaternik

Tea Rukavina

Fran Torbarina

Natalija Vitali

Andrija Vitlov

Filip Žugčić

SCIENTIFIC COMMITTEE:

Marko Čanadija

Vanja Travaš

Goran Vukelić

## Preface

My First Conference 2017 is a conference organized especially for the doctoral students and more ambitious graduate students of engineering and technology. It represents a joint initiative of Faculty of Civil Engineering, Faculty of Engineering and Faculty of Maritime Studies of the University of Rijeka. There are several reasons for the organizing of this conference:

- To provide the feedback to students for their ongoing research. Thus, presentations should not aim only at the completed research, but also at presenting research that is still not finished.
- The doctoral students will have a possibility to improve presentation skills at a scientific conference at no cost.
- It will connect young doctoral students from different institutions, and that should result in more interdisciplinary research projects,
- The international conference environment will be simulated by using the English as the conference language.
- Most doctoral students must publicly present research results of their research. This presentation can serve for this purpose.

Although the conference is organized primarily for the students of the University of Rijeka, students from other institutions are welcomed as well.

For the first conference, 2 keynote lectures and 29 contributed lectures were submitted. One keynote lecture will present author's rights in research publications, what is of interest not only to a doctoral student, but to their supervisors as well. The other keynote lecture will discuss brain-computer interface, a technology of utmost importance to handicapped people. Contributed lectures topics range from thermodynamics and mechanics, alternative energy sources, maritime problems, software engineering, electric vehicles and engineering in general.

For the first occasion, the conference takes place at the Faculty of Engineering, University of Rijeka. Conference co-chairmen hope that the conference will become an annual event, organized by the mentioned institutions employing the principle of rotation. In that way, the next conference is scheduled for the September 2018 at Faculty of Maritime Studies of the University of Rijeka.

Finally, the conference co-chairmen would like to thank all authors for submitting their contributions, as well as the supporting organizations for their help.

Rijeka, September 2017

Conference co-chairmen

Sandra Kvaternik, Fran Torbarina, Natalija Vitali

Marko Čanađija, Vanja Travaš, Goran Vukelić

## KEYNOTE LECTURES

I. Hreljac

*Authors' Rights in Scientific Publishing*

G. Madhale Jadav, L. Batistić, Saša Vlahinić and Miroslav Vrankić

*BCI communicator - A qualitative and quantitative analysis of the communication interface*

## CONTRIBUTED LECTURES

N. Anđelić, M. Čanadija, Z. Car

*Theoretical Investigation of Nanoelectromechanical Resonator for Detection of Nanoparticles Based on Simply Supported Single Layer Graphene Sheet using non-local theory of elasticity*

T. Arrigoni, S. Zelenika, E. Kamenar, T. Schnunner Luke Vrbanić, K. Lenac

*Issues in the Mechatronics Design of a Full Arm Rehabilitation Device*

L. Baić, B. Đurin

*Sizing of the Sustainable Irrigation System Driven by Solar Photovoltaic Energy and Wind by Using New Sizing Algorithm*

S. Baltic, A. Frohner, I. Stimac Grandic

*Determination of force coefficients for wind force calculation by Computational Fluid Dynamics*

D. Brusić, V. Travaš

*A Numerical Study of Kinematic Properties of the Flow inside Hydraulic Jumps*

S. Dobrilla, N. Čeh, G. Jelenić

*Experimental and numerical dynamic analysis of beam bridges subject to non-uniform seismic support excitation*

D. Glujić

*Fuel Cost Analysis In New Ship Propulsion Trends*

P. Gljušćić, S. Zelenika

*Modelling, optimization and application of piezoelectric vibration energy harvesting devices*

S. Grbac Babić, T. Galinac Grbac

*Community detection for software-systems in evolution*

S. Grbčić, G. Jelenić

*Finite element analysis of a linear elastic micropolar continuum: development of membrane elements with linked interpolation*

M. Jardas, K. Ivanić, P. Badurina Tomić

*Application of "Internet of things" in logistics processes*

M. Kirinčić, A. Trp

*Numerical Analysis of the Influence of Natural Convection on Melting and Solidification of Paraffin*

S. Kuzma, V. Travaš

*Physical Model of Discharge Structure at Rječina River near the Zvir Water Source*

S. Kvaternik, G. Turkalj, D. Lanc

*Numerical buckling analysis of thin-walled frames with joint effect*

F. Ledić, Z. Čarija, B. Ničeno

*Simulation of the turbulent fluid flow and mixing in a nuclear reactor model – ROCOM*

- R. Ljubek, A. Trp, K. Lenić  
*Numerical analysis of shell and tube heat exchanger*
- V. Medica-Viola, B. Pavković, V. Mrzljak  
*Coal-fired power plant condenser numerical model for on-condition monitoring*
- I. Pejić, V. Travaš  
*A Modern Replica of Darcy Experimental Apparatus & Experimental Study of Infiltration Dynamics*
- M. Perčić, S. Zelenika  
*Issues in characterizing parameters influencing nanometric friction*
- S. Piličić, M. Franulović, K. Marković  
*Procedure for modelling of soft tissues behavior*
- T. Rukavina, A. Ibrahimbegovic, I. Kozar  
*Modelling fibers in concrete using the XFEM methodology*
- F. Torbarina, K. Lenić  
*Heat Transfer Fluid Storage in the Solar Collection Loop - The Storage Volume Impact on the Work Performance of a Solar Absorption Cooling System*
- M. Tuhtan, G. Jelenić  
*Rocking of the block due to base movement*
- H. Vido  
*Shear design and diagonal crack control of reinforced concrete beams*
- N. Vitali, J. Prpić-Oršić  
*Ship Speed and Fuel Consumption: The Effect of Waves on Ship and Engine Dynamics*
- A. Vranković, T. Galinac Grbac  
*Preparation for replicating empirical study of a selection method for software reliability growth models*
- V. Vujnović  
*Light distribution for the calibration system in Muon  $g-2$  experiment - precise measurement which could lead to new physics*
- L. Zaharija, V. Travaš  
*Numerical Model of Natural Convection in the Artificial Lake Butoniga*
- F. Žugčić  
*Cost-effectiveness of electric vehicles*

# KEYNOTE LECTURES

# Authors' rights in scientific publishing

Hreljac Ivana<sup>1,\*</sup>

*<sup>1</sup>Hcewnm' qh'Gpi kpggt kpi . 'Wp'kxgt uk' qh'Tk'gnc*

E-mail: [ihreljac@riteh.hr](mailto:ihreljac@riteh.hr)

## 1 Introduction

In academia one of the main requirements for career advancement is publishing of research results in scientific journals. Scientific publishing allows scientists to share their work and provide other scientists with the research material. High subscription fees for scientific journals have become a rising problem because articles are not sufficiently accessible to the general public and scientific community. With reduced article visibility, authors are often encouraged to self-archive their accepted work. As authors usually must sign copyright transfer statement before publishing, it is necessary to investigate journal policies about self-archiving. Since there are always some restrictions, an idea of open access journals arose, where articles can be accessed by anyone, for free.

## 2 Authors' rights

Every original work in the literary, scientific and artistic domain is protected by author's rights as soon as it is created. Authors' rights don't protect ideas, discoveries, concepts, methods etc., only the way these are presented. Authors' rights consist of moral and economic rights. Moral rights consist of right of first publication, right to claim authorship, protection of a work's integrity and the right to object to the use of the author's work if future use would harm author's honour or reputation. Moral rights are granted only to the author of the work and are not transferable. In contrast to moral rights, economic rights can be sold or passed to the third party. Economic rights include right of reproduction, distribution, right to issue the work to the public and right of adaptation. When publishing in scientific journals, author must transfer economic rights to the journal which then has the legal right to publish, distribute and charge the article. [1,2]

### 2.2 Self-archiving and self-plagiarism

When the paper is ready for publication the publisher receives copyright for free (authors and reviewers are not compensated for their work) and sells subscriptions back to the universities who made the articles in the first place. Due to the high subscription prices this puts universities with smaller budget in an inferior position. [3] Thus authors are encouraged to self-archive articles in repositories or personal web pages to increase article visibility. The problem is an embargo – a period during which access to the academic journal is restricted without payment, thus restricting when and where an author can self-archive his work. This can cause infringement of copyright because authors are often not familiar with copyright transfer agreement which are different for every journal.

Self-archiving and self-plagiarism are one of the most common ways of copyright infringement. Plagiarism is considered presenting someone else's work as if it is their own

\* Corresponding author

without proper citation and presenting work that is derived from existing one as an original work. After the article publication, authors may have the opportunity to continue their research which could result with a new article. Authors may consider that they can reuse parts of their work in the new article without including citations to the original work, believing they are not plagiarizing someone else's work since it is their own. But the second part of plagiarism definition is often overlooked, where they present an old idea or work as a new one. [4]

### 3 Open Access

Open access journals publish articles that are free for everyone as soon as they are published. Many open access projects and initiatives provide support for universities and authors to improve discoverability and reusability of research publications. To understand importance of open access, a call from EU Competitiveness Council can be pointed out where it was stated that all scientific papers should become open access by 2020. [5]

The main problem with open access publishing is that the scientists have to pay publishing fees which are often too expensive. Because of the publication payment, journals accept greater amount of papers than subscription based journals which can reduce the quality of a journal. Many authors still prefer sending their manuscripts to subscription based journals which are more recognized than open access ones. [6]

Publishing in open access is done under Creative Commons licences. There are six licences which combine conditions of sharing, attribution, commercial usage and derivations of work. Author can choose which one he wants to prohibit or allow. As an addition, author can give work to the public domain with no rights reserved. [7]

### 4 Conclusion

Scientists must be familiar with the authors' rights and what happens to them when publishing in a scientific journal. Most common situations when authors violate copyright, sometimes even without knowing, are self-archiving and self-plagiarism. There is a growing criticism of the high subscription cost which led to the idea of open access. Open access allows for greater dissemination of scientific material, increased visibility and citation of material. Despite some disadvantages there is a number of initiatives and projects that provide education and support scientists to archive their work to make them publicly available and permanently saved from loss.

### References

- [1] Autorski registar. *O autorskim pravima*. [www.autorski-registar.com](http://www.autorski-registar.com). Accessed 2016.
- [2] DZIV. *Autorsko pravo i srodna prava*. [www.dziv.hr](http://www.dziv.hr). Accessed 2016.
- [3] Taylor Michael P., 2012. *Opinion: Academic Publishing is broken*. [www.the-scientist.com](http://www.the-scientist.com). Accessed 2016.
- [4] Ithenticate – white book. *The ethics of self-plagiarism*, [www.ithenticate.com](http://www.ithenticate.com), Accessed 2016.
- [5] Martin E. *In dramatic statement, European leaders call for 'immediate' open access to all scientific papers by 2020*. [www.sciencemag.org](http://www.sciencemag.org). Accessed 2016.
- [6] Eveleth R. *Free Access to Science Research Doesn't Benefit Everyone*. [www.TheAtlantic.com](http://www.TheAtlantic.com). Accessed 2016.
- [7] Creative Commons. *About licences*. <https://creativecommons.org>. Accessed 2016.

# BCI communicator - A qualitative and quantitative analysis of the communication interface

Guruprasad Madhale Jadav, Luka Batistić, Saša Vlahinić and Miroslav Vrankić  
Tehnički Fakultet Sveučilište u Rijeci, Rijeka, Croatia

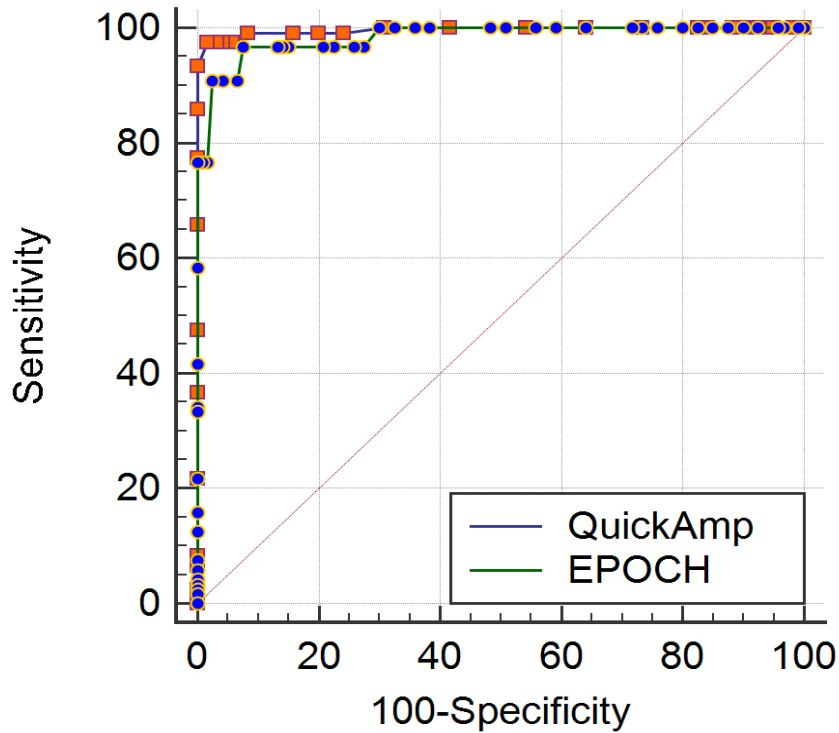
jguruprasad@riteh.hr

## **Abstract**

The brain computer interface (BCI) communicator system is built using technology which measures electroencephalography (EEG), this is done when a user is actively listening to all the auditory stimuli and responding to the desired stimulus. This principle of response to stimulus produces a P300 event related potential (ERP), which is nothing but the change in electric potential due to the event. This auditory ERP of interest was compared considering different type of stimuli and different methods of responses to these stimuli, also parameters like different kind of users, from healthy people to people in locked-in state and the results of each such user group, and comparison of accuracy of visual P300 system with an auditory system gave us a quantitative measure of the performance of BCI communicator. Such an analysis enables to deduce the performance metrics of the system to conclude the usability of such a system in real world scenario. The EEG recording hardware plays an important role for everyday use case and thus we choose a low cost, easy to use hardware called Emotiv EPOC. The evaluation of quantitative and qualitative parameters of such a hardware becomes crucial to understand the potential and limitations of it, this is done by comparing its performance with laboratory grade EEG recording device like QuickAmp.

## **Hardware Performance Analysis**

The BCI communicator experiment, is conducted to analyze the performance of the two devices that were used to measure the EEG data of subjects who participated in the experiment.



### Comparison of ROC curves

Variable 1	QuickAmp
Variable 2	EPOCH
Classification variable	TP/FP
Sample size	240
Positive group <sup>a</sup>	120 (50.00%)
Negative group <sup>b</sup>	120 (50.00%)

<sup>a</sup> TP = 1

<sup>b</sup> FP = 0

Variable	AUC	SE <sup>a</sup>	95% CI <sup>b</sup>
QuickAmp	0.996	0.00254	0.978 to 1.000
EPOCH	0.983	0.00601	0.958 to 0.995

<sup>a</sup> DeLong et al., 1988

<sup>b</sup> Binomial exact

### Pairwise comparison of ROC curves

QuickAmp ~ EPOCH	
Difference between areas	0.0128
Standard Error <sup>a</sup>	0.00659
95% Confidence Interval	-0.0000676 to 0.0258
z statistic	1.950
Significance level	P = 0.0512

<sup>a</sup> DeLong et al., 1988

During the experiment, the subjects had to select the correct answer to the asked question by mentally counting it, this mental counting created P300 response to stimulus which was expected to be only visible for the correct answer. The true positive (TP) and false positive (FP) value for every such experiment were calculated.

The obtained true positive and false positive values for both QuickAmp and Emotiv EPOC were used for analysis of area under the curve. The classification variable in the data for analysis voted 1 for TP data and 0 for FP data, thus allowing the calculation of true positive rate and false positive rate which is nothing but sensitivity and (1-specificity) respectively.

The confidence interval for both QuickAmp and EPOC being more than 0.9 assures that the ROC curve analysis results are reliable. The significance level or P-value for pairwise comparison of ROC curves is 0.0512 which is above the lower threshold ( $\alpha = 0.05$ ) which proves that they are significantly different. This is expected as the EEG data recorded and amplified by the QuickAmp is of higher quality.

The area under the curve which is 99.6 % for QuickAmp signifies that it has 1.3 % AUC than 98.3 % of Emotiv EPOC, which shows that with QuickAmp we have slightly better classification accuracy.

## **Conclusion**

As the results show, the classification accuracy of QuickAmp does not drastically vary from Emotiv EPOC. But QuickAmp hardware has restricted usability due to cost and setup requirements. Allowing us to choose Emotiv EPOC has our primary recording device.

# CONTRIBUTED LECTURES

# Theoretical Investigation of Nanoelectromechanical Resonator for Detection of Nanoparticles Based on Simply Supported Single Layer Graphene Sheet using Non-local Theory of Elasticity

Nikola Anđelić\*, Marko Čanadija, Zlatan Car

<sup>1</sup>Faculty of Engineering Rijeka, Vukovarska 58 51000 Rijeka  
E-mail: [nandelic@riteh.hr](mailto:nandelic@riteh.hr)

<sup>2</sup>Faculty of Engineering Rijeka, Vukovarska 58 51000 Rijeka  
E-mail: [markoc@riteh.hr](mailto:markoc@riteh.hr)

<sup>3</sup>Faculty of Engineering Rijeka, Vukovarska 58 51000 Rijeka  
E-mail: [car@riteh.hr](mailto:car@riteh.hr)

## 1 Introduction

Due to its extraordinary mechanical, electrical and thermal properties graphene sheets have many potential applications such as reinforced materials, molecule sensors and nanoelectromechanical resonators [1]. Nowadays a lot of resources and effort is focused on extensive research for possible application of graphene sheets in high-performance hybrid supercapacitors, optoelectronic devices and various types of high performance sensors. Nanoelectromechanical systems or shortly NEMS are strong candidates for variety of applications in semiconductor-based technology and fundamental science [2]. NEMS resonators are used as the precision mass sensors which are used to weigh cells, biomolecules, and gas molecules [3,4,5]. NEMS mass sensor relies on monitoring how the resonance frequency of a NEMS resonator changes when an additional mass is absorbed onto its surface.

In this paper the vibrations of simply supported graphene sheet with and without attached nanoparticle is analysed using nonlocal plate theory. After the derivation of equation which describes the vibrations of simply supported SLGS the influence of nonlocal parameter and nanoparticle mass (attached to the GS) on vibrations of SLGS is analysed and results graphically represented.

## 2 Determination of resonant frequencies of simply supported SLGS

In this paper the dynamic behaviour of single layer graphene sheet or shortly SLGS with attached concentrated mass  $m_c$  located at an arbitrary position  $(x_0, y_0)$  is considered using nonlocal continuum mechanics and the schematic illustration of the problem is shown in the following figure.

---

\* Nikola Anđelić

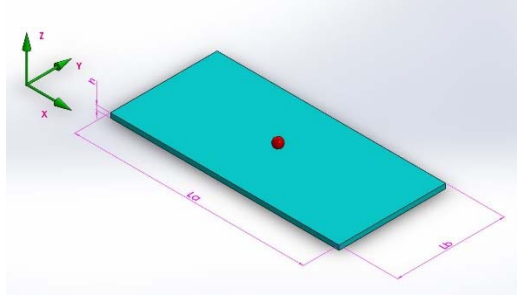


Fig.1. Schematic illustration of SLGS with attached mass at arbitrary position

Since the SLGS is simply supported the following boundary conditions are applied:

$$w = 0, \frac{\partial^2 w}{\partial x^2} = 0, \frac{\partial^2 w}{\partial y^2} = 0 \text{ on } x = 0, L_a, \text{ and } y = 0, L_b \quad (1)$$

The expression for determining resonant frequencies can be written in the following form

$$\omega_{mn}^2 = \frac{D\pi^4 \left( \frac{m^2}{L_a^2} + \frac{n^2}{L_b^2} \right)^2}{\left[ 1 + (e_0 a)^2 \pi^2 \left( \frac{m^2}{L_a^2} + \frac{n^2}{L_b^2} \right) \right] \left( \rho h + \frac{4m_c}{L_a L_b} \sin^2 m\pi\xi \sin^2 n\pi\eta \right)} \quad (2)$$

It's worth mentioning that when the nonlocal parameter  $e_0 a$  is equal to zero, the resonant frequency of SLGS with attached nanoparticles can also be obtained from classical plate theory.

### 3 Results and discussion

As mentioned before in these simulations, the nanomechanical resonator is considered which consist of simply supported graphene sheet with attached nanoparticle. Geometrical and mechanical data of simply supported graphene sheet is shown in Tab. 1.

Tab.1 Geometrical and mechanical characteristics of SLGS [1,2]

Description	Value
Length [nm]	150
Width [nm]	75
Thickness [nm]	0.127
Internal characteristic length [nm]	1.42
Modulus of elasticity [TPa]	2.81
Density [kg/m <sup>3</sup> ]	2300
Poisson's number	0.149

The Fig.2 shows three curves and each curve represents simulation with different nonlocal parameter (0.0, 1.0 and 2.0 nm).

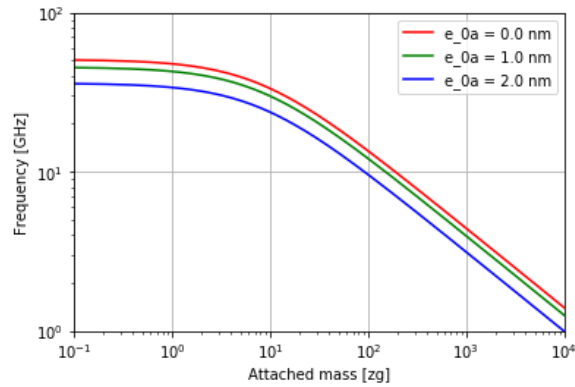


Fig. 3 Variation of the resonant frequency in SLGS as a function of attached mass for different nonlocal parameters. ( $m = n = 1, \xi = 0.5, \eta = 0.5$ )

#### 4 Conclusion

The nonlocal plate theory as mentioned before, is just extension of classical plate theory used to tackle problems at nanoscale. The results showed that the nonlocal parameter has a huge influence on resonant frequencies of simply supported SLGS. When the value of nonlocal parameter gets larger it lowers the resonant frequency. The investigation also showed that a mass of attached nanoparticle has huge influence on resonant frequencies of simply supported SLGS. As the mass of the attached nanoparticle increases the resonant frequencies becomes lower.

#### References

- [1] Natsuki, I. 2015. Theoretical Analysis of Vibration Frequency of Graphene Sheet Used as Nanomechanical Mass Sensor. *Electronics*, 4, pp. 723-738.
- [2] Natsuki, T., Shi, J.-X. and Ni, Q.-Q., 2013. Vibration Analysis of Nanomechanical Mass Sensor Using Double-Layered Graphene Sheet Resonators. *Journal of Applied Physics*, 114, pp. 1-5.
- [3] Naik, A.K., Hanay, M.S., Hiebert, W.K., X.L., Feng, X.L. and Roukes M.L., 2009. Towards Single-Molecule Nanomechanical Mass Spectrometry. *Nature Nanotechnology* 4, pp. 445-450.
- [4] Jensen, K., Kim, K. and Zettl, A. 2008. An Atomic-Resolution Nanomechanical Mass Sensor. *Nature Nanotechnology* 3, pp. 533-537.
- [5] Burg, T.P., Godin, M., Knudsen, S.M., Shen, W., Carlson, G., Foster, J.S., Babcock, K., and Manalis R.S., 2007. Weighing of Biomolecules, Single Cells and Single Nanoparticles in Fluid. *Nature* 446, pp. 1066-1069.

# Issues in the mechatronics design of a full arm rehabilitation device

T. Arrigoni,<sup>1,2,\*</sup> S. Zelenika,<sup>1,2</sup> E. Kamenar,<sup>1,2</sup> T. Schnurrer Luke Vrbanić<sup>3</sup>  
and K. Lenac<sup>1</sup>

<sup>1</sup> University of Rijeka, Faculty of Engineering, Vukovarska 58, 51000 Rijeka, CROATIA

<sup>2</sup> University of Rijeka, CMNST, Radmile Matej i 2, Rijeka, CROATIA

<sup>3</sup> U. of Rijeka, School of Medicine, Braće Branchetta 20, 51000 Rijeka, CROATIA

E-mail: [tea.arrigoni@gmail.com](mailto:tea.arrigoni@gmail.com), [sasa.zelenika@riteh.hr](mailto:sasa.zelenika@riteh.hr)

## 1 Introduction

Stroke is the leading cause of adult disability in western countries. Impairments in movements are among the most common consequences of stroke, while upper limb functions are altered in up to 75 % of the patients [1]. Traditional therapy for the recovery of patients with arm impairments involves physical therapists that control the movements and help the patients recover the motion ability. The limited number of physiotherapists and of their time availability constitute here an increasing problem. In the last decades, robotic-based rehabilitation devices have thus become common. These can have a varying number and arrangement of DOFs that influence the ease of movement but also the size, weight and price of the device [2]. The aim of this work is, hence, to perform an initial evaluation of the issues in the mechatronics design of a full arm rehabilitation device in order to find an optimal and highly efficient solution at a reasonable cost.

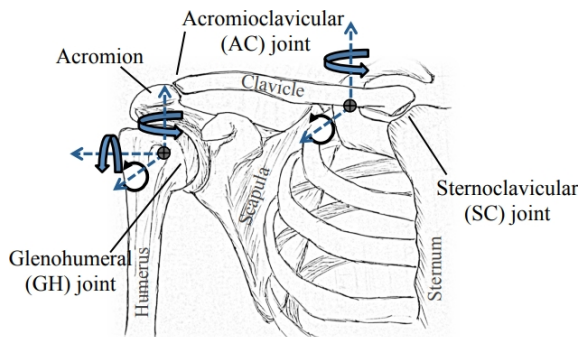


Fig. 1. Human arm [3]

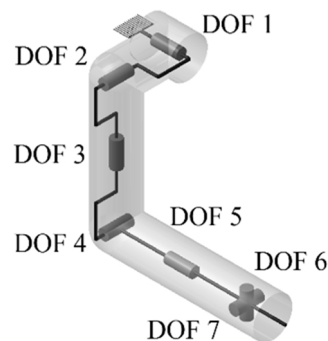


Fig. 2. The 7 DOFs model of the arm

## 2 Human Arm Behaviour and Respective Mechatronics Components

A crucial task in designing an arm rehabilitation device is the study of the arm's movement kinematics (Fig. 1). The human arm and the respective rehabilitation device are commonly modelled in literature as a 5-7 (and even up to 11) DOFs system [2]. Analysing then in depth the rehabilitation devices currently available on the market, it is concluded that the 7 DOFs models provide a good combination of motion accuracy with an acceptable model complexity (Fig. 2); this configuration is thus chosen for the design of the herein considered active rehabilitation device. The active part of this device is whence considered as a system with several sets of the three main hardware components,

\* Corresponding author

i.e., the actuators, the sensors and the control unit. In fact, the actuators should provide the needed help to the patients while performing the motions otherwise not achievable by their own, while the sensors should provide the needed feedback to the used control system so as to optimize the level of help when the patients' autonomy level is reached.

The commonly used types of actuators used in arm rehabilitation devices and their main characteristics are evaluated in Tab. 1. It is to be noted here that DC and servomotors use electricity and thus generate heat, whereas pneumatic motors make a lot of noise. Hydraulic motors are quiet but they and the pneumatic motors can generate problems related to leakages and often require a lot of space. On the other hand, the most commonly used sensors in arm rehabilitation devices and their features are listed in Tab. 2. Clearly, the position sensors should be of the absolute type so as to be ready at power up.

Tab. 1. Actuators and their main characteristics

	Pneumatic	Hydraulic	Servomotor	DC motor	Muscle (hydraulic)
Power	Middle	Very high	Low	Middle	High
Velocity	High	High	High	Low	High
Flexibility	High	Middle	High	Low	High
Price	Low	High	Very high	High	Middle
Efficiency	Low	Middle	High	High	Low

Tab. 2. Sensor types and their characteristics

	MEMS inertial	Magnetic angular	Capacitive	Torque	Pressure & touch	Electromyography
Measurement type	Displ., direction, orient.	Joints' angles	Force	Joints' torque	Pressure	Muscle activation
Dimensions	↓↓	↓	↓↓ ... ↑↑	↑	↓	↓
Price	High	Low	High	Middle	Middle	Middle

### 3 Conclusions and Outlook

Considerations about the number and arrangement of DOFs and of the usable actuators and sensors complement the performed initial critical evaluation of the configuration to be adopted in designing the mechanics of an efficient full arm rehabilitation device at a reasonable cost. Obviously, a proper choice of the other components (power supply, gearheads and similar) should also be performed bearing in mind the overall weight and needed floor space of the overall device. The configuration of the respective computing part controlling the performances of the complete mechatronics device, complemented ideally with a virtual reality users' interface that allows following patients' improvements and stimulating them to make full use of their efforts, will allow completing the layout of the considered device. It should finally provide the rehabilitation treatment with high intensity and frequency and support the rehabilitation of both the left and the right arm.

### References

- [1] Ovbiagele, B. and Nguyen-Huynh, M. N., 2011. *Neurotherapeutics*, 8(3), pp. 319-329.
- [2] Kim, H., 2012. D. Sc. thesis, U. California Santa Cruz.
- [3] Deshpande, A. D., 2015. Two Exoskeletons for Upper-Body Rehabilitation, U. Texas Austin.

# Sizing of the Sustainable Irrigation System Driven by Solar Photovoltaic Energy and Wind by Using New Sizing Algorithm

Lucija Baić<sup>1,\*</sup>, Bojan Đurin<sup>2</sup>

<sup>1</sup>Faculty of Geotechnical Engineering, University of Zagreb  
E-mail: name: lucija.baic@gmail.com

<sup>2</sup>Faculty of Geotechnical Engineering, University of Zagreb  
E-mail: bojan.djurin@gfv.hr

## 1 Introduction

Using of renewable energy sources in irrigation systems nowadays is very important, due to reducing the use of fossil fuels and due to negative effects of climate changes. This paper presents a new sizing methodology for an irrigation system driven by solar photovoltaic (PV) energy and wind energy with regards to critical period(s). This kind of methodology hasn't been presented so far. The analyzed irrigation system consists of four subsystems: subsystem PV (photovoltaic subsystem), subsystem W (wind system), subsystem R (water reservoir) and subsystem P (pump station). For each subsystem, critical period(s) will be defined:  $t_{PV}^*$ ,  $t_W^*$ ,  $t_R^*$  and  $t_P^*$ . Also, this paper will present two possible combinations for powering the irrigation system. In the first one, PV energy is the main source of energy and the Wind system is a backup, while in the second variant the Wind energy is the main source and the PV system is a backup.

## 2 Methodology

### 2.1 Definition of the critical day ( $t_{PV}^*$ , $t_W^*$ , $t_R^*$ and $t_P^*$ )

Critical period method [1] and [2] includes design elements of the solution: PV system, wind system, pump station and water reservoir based on the critical period of operation of each one. The balancing period of water pumping and water reservoir, water balance, is usually at least one day and may be several days, usually no more than five, ( $t_b = 1$  till 5 days). The minimum required power for subsystem PV is determined from established differences  $\Delta V_{tb,i}$  [2]:

$$\Delta V_{tb,i} = V_{P,tb,i} - V_{daily,tb,i} \quad (1)$$

where  $V_{P,tb,i}$  is daily amount of water pumped into the water reservoir at a certain time/period (day)  $i$  and  $V_{daily,tb,i}$  is required daily amount of water for the irrigation needs.

The critical day/period for PV generator design is determined by statistical minimization, where  $\Delta V_{tb,i}$  is a difference which is typically equal to 0:

$$\min \Delta V_{tb,i} \Rightarrow t_{PV,tb,i}^* \quad (2)$$

\*Corresponding author

On same manner, critical period  $t_W^*$  for subsystem W can be calculated, but for this case with different denotation, i.e.  $P_W$ .

For the subsystem R (reservoir), the required volume  $V^*$  for each variant  $t_b$  is obtained using statistical maximization, with the associated critical day [2]:

$$V^* \geq \max V \Rightarrow t_{R,tb,i}^* \quad (3)$$

The critical day for the sizing of the subsystem P, considering PV energy, refers to the day in which the daily duration of solar radiation  $T_s$ , which is suitable for pumping, is shortest during the analyzed year. The critical day for the sizing of the subsystem P, considering wind energy, refers to the day in which the daily wind speed  $W_s$ , which is suitable for water pumping, is longest during the analyzed year.

The same situation applies to the capacity of pump stations  $Q_p^*$  [2]:

$$Q_p^* \geq \max Q_p \Rightarrow t_{P,tb,i}^* \quad (4)$$

## 2.2 Optimization combinations (options A and B)

For this research, two combinations are suggested:

- A) PV energy is main source of energy, Wind energy is backup.
- B) Wind energy is main source of energy, PV is backup.

These two combinations allow the use of the mentioned sizing methodology on different locations in the world, bearing in mind that for some locations the wind energy will be better suited than the PV energy and vice versa.

## 3 Conclusion

This methodology will be tested on small scale [3] and large scale projects [4]. Small scale project will be applied for irrigation of football field in Sveti Ilija, near Varaždin in Croatia, which is mentioned and described in [3]. Large scale project will be applied in Decan, Kosovo described in [4]. It is expected that irrigation system sized by Critical period method is more energy and hydraulically efficient than irrigation system sized by traditional method.

## References

- [1] Đurin, B. and Margeta, J., 2014. Analysis of the possible use of solar photovoltaic energy in urban water supply systems. *Water*, 6, pp.1546-1561.
- [2] Đurin, B., 2014. Sustainability of the urban water supply system operating. PhD thesis. Faculty of Civil Engineering, Architecture and Geodesy, University of Split, Split, Croatia (in Croatian).
- [3] El-Shimy, M. and Đurin, B., 2016. Techno-economic evaluation and sizing optimization of solar-PV and wind energy sources for irrigation water pumping. *Energy and the Environment*, pp. 209-220.
- [4] Lajqi, S., Đurin, B., Baić, L., Doci, I., Lajqi, N., Drilon, M., 2017. Critical Period Method - Innovative Method for Sizing of the Irrigation Systems: Case Kosovo. *Mechanization in Agriculture & Conserving of The Resources*, 63 (4), pp. 157-160.

# Determination of force coefficients for wind force calculation by Computational Fluid Dynamics

Sandra Baltić<sup>1,\*</sup>, Andreas Frohner<sup>2</sup>, Ivana Štimac Grandić<sup>2</sup>

<sup>1</sup>Faculty of Civil Engineering Rijeka, Radmile Matejčić 3, 51000 Rijeka, Croatia  
E-mail: [sandra.baltic@student.uniri.hr](mailto:sandra.baltic@student.uniri.hr), [istimac@gradri.uniri.hr](mailto:istimac@gradri.uniri.hr)

<sup>2</sup>University of Natural Resources and Life Sciences, Institute of Chemical and Energy Engineering, Muthgasse 107, 1190 Vienna, Austria  
E-mail: [andreas.frohner@boku.ac.at](mailto:andreas.frohner@boku.ac.at)

## 1 Introduction

The calculation of wind load is based on estimates of wind effects, which must be taken into account in the design of structure. The wind force for a structural element can be determined directly, employing the procedure which incorporates aerodynamic information, from the following expression [1]:

$$F_w = c_s c_d \cdot c_f \cdot q_p(z) \cdot A_{ref} \quad (1)$$

where  $c_f$  is the force coefficient which defines aerodynamic effects of the wind loads,  $c_s c_d$  is the structural factor,  $q_p(z)$  is the peak velocity pressure and  $A_{ref}$  is the reference area. The Eurocode defines force coefficient  $c_f$  as follows [1]:

$$c_f = c_{f,0} \cdot \Psi_r \cdot \Psi_\lambda \quad (2)$$

where  $c_{f,0}$  is the basic value,  $\Psi_r$  is reduction factor which counts on rounded corners,  $\Psi_\lambda$  is the end-effect factor for elements with free-end flow.

Computational Fluid Dynamics (CFD) enables engineers to perform “numerical experiments” in a “virtual flow laboratory”. In this study, basic value of force coefficient  $c_{f,0}$  which depends on the shape of cross-section is analysed using ANSYS Fluent, together with reduction factor  $\Psi_r$  which counts on beneficial effects of rounded edges.

## 2 Application of CFD

Bridge piers with different cross-sections are investigated for the purpose of finding aerodynamic information. The width exposed to wind is  $b=1$  m. The length along the wind direction is noted as  $d$ . All piers are 20 m high. Analysed geometry is shown in Fig. 1.

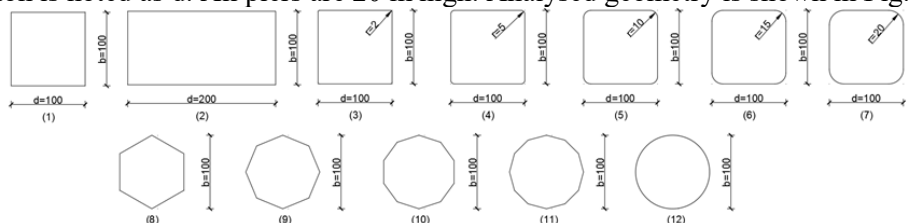


Fig. 1. Cross-section geometry of analysed bridge piers (measures in cm)

\* Corresponding author

User Defined Function (UDF) is assigned at the inlet face of model to simulate atmospheric boundary layer. Velocity profile corresponds to mean wind velocity for terrain category II defined by [1] and represents the roughness characteristics of the terrain, which have to be included in computational domain. Standard k- $\omega$  model is employed for modelling turbulence. Details about adopted domain size, meshing customization, boundary conditions and solver settings can be found in [2].

Total drag force component is wanted solution from simulation. The total force on a wall zone (pier) is computed in ANSYS Fluent by summing pressure and viscous forces. To render wind forces dimensionless, the associated force coefficients are computed using the reference values. The force coefficient is defined as follows [3]:

$$c_f = \frac{1}{2} \cdot \rho \cdot v^2 \cdot A \quad (3)$$

where  $\rho$ ,  $v$  and  $A$  are the density, velocity and area, specified in Reference Values. The following are used for all computations:  $\rho = 1.25 \text{ kg/m}^3$ ,  $v = 25.5 \text{ m/s}$ ,  $A = 20 \text{ m}^2$ .

### 3 Results and discussion

Simulation results for rectangular, rounded and polygonal sections are shown in Fig. 2. and compared with Eurocodes values. It can be seen that the solutions are physically consistent and within reasonable ranges. Force coefficient of circular section obtained from CFD simulation is 0.936 (0.798 according to EN procedure). This relative difference of 17% for circular shape is the largest one and it is exception since all other solutions deviate for less than 10%.

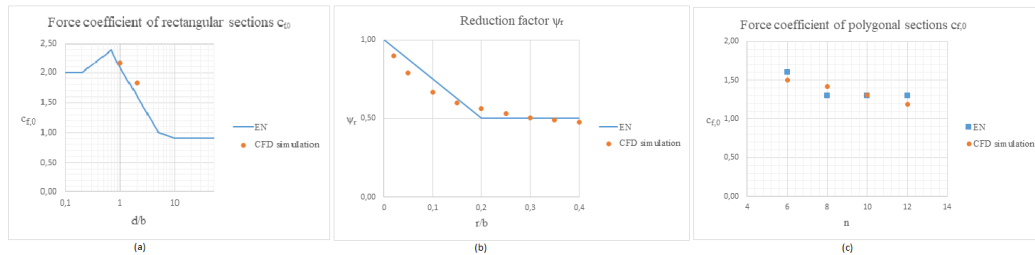


Fig. 2. Simulation results: (a-force coefficient for square and rectangular section, b-reduction factor for rounded corners depending on  $r/b$  ratio where  $r$  is curvature radius, c-force coefficient for polygonal sections depending on number of sides  $n$ )

### 4 Conclusion

Application of CFD for investigation of aerodynamic response of structural elements proved to be justified. Numerical simulations allow finding force coefficients for arbitrary form not available in standard without expensive wind experiments.

#### References

- [1] EN 1991-1-4, Eurocode 1 – Actions on structures: Part 1-4: General actions – Wind actions, CEN, Bruxelles, 2005.
- [2] Baltić, S.: Determination of force coefficients for wind force calculation by Computational Fluid Dynamics, Master's Thesis, 2017.
- [3] ANSYS Fluent Theory Guide, Release 18.0, SAS IP, U.S.A., 2016.

# Numerical Study of Kinematic Properties of the Flow Inside Hydraulic Jumps

Daniel Brusić<sup>1,\*</sup>, Vanja Travaš<sup>1</sup>

<sup>1</sup>Faculty of Civil Engineering, University of Rijeka, Radmile Matejčić 3, 5100 Rijeka  
E-mail: [daniel.brusic@student.uniri.hr](mailto:daniel.brusic@student.uniri.hr), [vanja.travas@gradri.uniri.hr](mailto:vanja.travas@gradri.uniri.hr)

## 1 Introduction

A hydraulic jump is a phenomenon which describes a jump or standing wave formed when the flow regime changes from a supercritical flow to a subcritical flow. Although its characteristics are very well documented [1,2], they are mostly based on experimental data. The aim of this paper is to better understand the characteristics of a hydraulic jump through a numerical model analysis. This approach allows us to see a detailed view of the structure of the hydraulic jump and the field of relevant kinematic properties. A lot of effort was put into the parametric analysis of the flow when comparing different wall roughness settings and the effect it has on relevant parameters within the hydraulic jump.

## 2 Model description

### 2.1 Geometry and mesh

The geometry of the model is based upon a part of the hydraulic channel located in the Hydraulic Engineering lab in the building of the Faculty of Civil Engineering Rijeka.

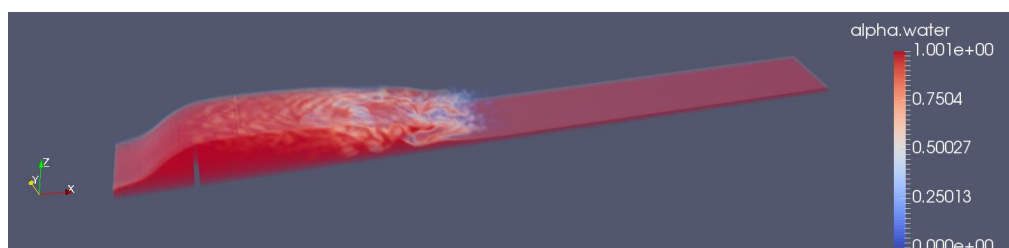


Fig. 1. The domain – water/air distribution calculated for 0 mm roughness and  $t=40$  s

The dimensions of the domain are:  $L=320$ cm,  $B=31$ cm and  $H=40$ cm and the whole domain is tilted at 2% in the negative x-axis direction. To invoke a hydraulic jump, a step is positioned near the outlet of the model. The mesh is a hexahedral mesh and it consists of 657 820 hexahedra.

### 2.2 Numerical model

In order to simulate flow inside the domain appropriate software had to be used. OpenFOAM was selected to run the simulation with the main reason for choosing it that it is an open source software, unlike most of its competitors. OpenFOAM offers a plethora

\* Corresponding author

of different solvers but for this case the *interFoam* solver was chosen. It is a solver for 2 incompressible fluids and is based on the volume of fluid method. This means that in our model we have water and air and the interaction of these 2 phases is calculated through the *interFoam* solver. The  $k-\varepsilon$  turbulent model was used to simulate the dissipation of energy caused by the viscous forces and to approximate the turbulent structure of the flow.

### 2.3 Boundary and initial conditions

Appropriate application of the  $k-\varepsilon$  wall function parameters was applied to simulate the wall roughness. The inlet is on the right side and the inlet speed of water is 3m/s in the negative x-axis direction. All the other surfaces are atmospheric so it allows water and air to exit the domain.

## 3 Results and conclusion

In order to compare kinematic properties of hydraulic jumps a method was devised to analyse the jump characteristics. The domain was divided into a large number of slices and then the mean height and velocity for each slice was extracted. From that the  $Fr$  number was calculated and displayed on the same graph. An example can be seen on Fig 2..

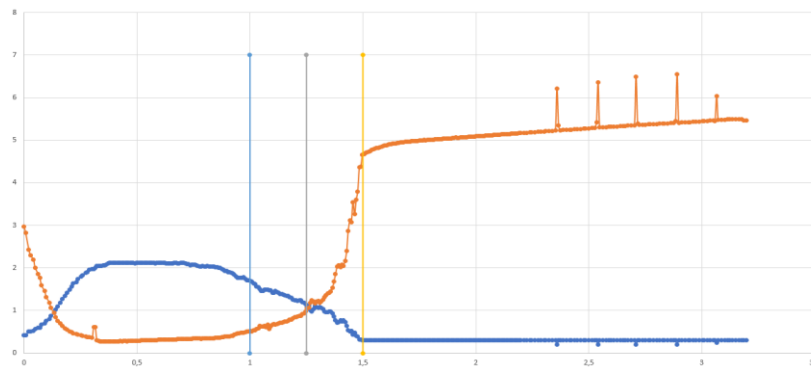


Fig. 2. Mean water level (blue) displayed with  $Fr$  number (orange) for roughness of 0 mm and  $t=60$  s – vertical lines represent the hydraulic jump

Further research is needed to make the connection between wall roughness and the kinematic properties of jumps but preliminary results show that higher roughness causes the jump to move more away from the step and the overall length of the jump becomes smaller. Usually empirical equations don't factor in the effect of wall roughness when predicting kinematic properties of a jump but based on the data in this paper we can see that it makes a significant difference.

## References

- [1] Gandhi S., 2014. *Characteristics of Hydraulic Jump*, World Academy of Science, Engineering and Technology
- [2] Neluwala N.G.P.B., Kurunanayake K.T.S., Sandaruwan K.B.G.M., Pathirana K.P.P., 2013., *Characteristics of Hydraulic Jumps over Rough Beds – An Experimental Study*, ENGINEER – Vol. XXXXVI, No 03 pp. [1-7]

# Experimental and numerical dynamic analysis of beams subject to non-uniform seismic support excitation

Nina Čeh\*, Simona Dobrilla, Gordan Jelenić

*Faculty of Civil Engineering, University of Rijeka*

E-mail: [nina.ceh@uniri.hr](mailto:nina.ceh@uniri.hr), [simona.dobrilla@student.uniri.hr](mailto:simona.dobrilla@student.uniri.hr), [gordan.jelenic@uniri.hr](mailto:gordan.jelenic@uniri.hr)

## 1 Introduction

In earthquake-prone regions, the principal problem of structural dynamics is the behaviour of structures subject to multi-support excitation. In larger structures with greater distance between the supports, such excitation may become non-unique, which plays an important role in their safety and durability. These effects may result in structural failure due to excessive relative displacements between the supports [1].

## 2 Analytical approach

### 2.1 Dynamic response of a multi-degree-of-freedom system (MDOF)

For structures subject to earthquake induced multi-support excitation, the displacement vector contains two parts: the vector of total displacements  $\mathbf{u}_t$  involving the unknown degrees of freedom, and the vector  $\mathbf{u}_g$  of the known support displacements. The dynamic equilibrium equation in that case can be written as [1]

$$\begin{bmatrix} \mathbf{m} & \mathbf{m}_g \\ \mathbf{m}_g^T & \mathbf{m}_{gg} \end{bmatrix} \begin{Bmatrix} \ddot{\mathbf{u}}_t \\ \ddot{\mathbf{u}}_g \end{Bmatrix} + \begin{bmatrix} \mathbf{c} & \mathbf{c}_g \\ \mathbf{c}_g^T & \mathbf{c}_{gg} \end{bmatrix} \begin{Bmatrix} \dot{\mathbf{u}}_t \\ \dot{\mathbf{u}}_g \end{Bmatrix} + \begin{bmatrix} \mathbf{k} & \mathbf{k}_g \\ \mathbf{k}_g^T & \mathbf{k}_{gg} \end{bmatrix} \begin{Bmatrix} \mathbf{u}_t \\ \mathbf{u}_g \end{Bmatrix} = \begin{Bmatrix} \mathbf{0} \\ \mathbf{p}_g(t) \end{Bmatrix}, \quad (1)$$

where  $\mathbf{m}$ ,  $\mathbf{m}_g$ ,  $\mathbf{m}_{gg}$ ,  $\mathbf{c}$ ,  $\mathbf{c}_g$ ,  $\mathbf{c}_{gg}$  and  $\mathbf{k}$ ,  $\mathbf{k}_g$ ,  $\mathbf{k}_{gg}$  are submatrices of the mass, damping and stiffness matrices related to the two parts of the displacement vector and their first and second time derivatives  $\dot{\mathbf{u}}_t$ ,  $\dot{\mathbf{u}}_g$ ,  $\ddot{\mathbf{u}}_t$ ,  $\ddot{\mathbf{u}}_g$ , and  $\mathbf{p}_g(t)$  are the support reactions.

Separating the vector of total displacements into the part that refers to structural displacements due to a static application of the support displacements and the part that refers to relative displacements  $\mathbf{u}$ , the equation of motion for MDOF systems becomes

$$\mathbf{m}\ddot{\mathbf{u}} + \mathbf{c}\dot{\mathbf{u}} + \mathbf{k}\mathbf{u} = \mathbf{p}_{eff}(t) \quad (2)$$

where the vector of effective earthquake forces  $\mathbf{p}_{eff}(t)$  is equal to [1]

$$\mathbf{p}_{eff}(t) = (\mathbf{m}\mathbf{k}^{-1}\mathbf{k}_g - \mathbf{m}_g)\ddot{\mathbf{u}}_g(t) + (\mathbf{c}\mathbf{k}^{-1}\mathbf{k}_g - \mathbf{c}_g)\dot{\mathbf{u}}_g(t). \quad (3)$$

### 2.2 Modal analysis

For the  $n$  DOF system, calculating a dynamic response includes solving the set of  $n$  coupled differential equations which is rather complex. To find the dynamic response of

\* Corresponding author

linear MDOF systems, a procedure called modal analysis comes as useful, whereby a transformation matrix  $\Phi$  may be utilized to express the relative displacements  $\mathbf{u}$  in terms of the modal coordinates as  $\mathbf{u} = \Phi \mathbf{Y}$ . In this way the mass, stiffness and damping matrices (with Rayleigh damping assumed) become diagonal and the set of  $n$  coupled differential equations is transformed into the set of  $n$  uncoupled differential equations in modal coordinates which are easy to solve [1].

### 3 Numerical approach

In practice, the dynamic excitation is not harmonic, but rather arbitrarily changing in time. If the earthquake record is given by an acceleration-time history input, the resulting uncoupled differential equations may not be solved analytically. Instead, a numerical approach should be applied, in which the total response time is divided into a finite number of intervals in which the vector of the effective earthquake forces is approximated as linearly changing. For the known acceleration at the beginning and at the end of each interval, using numerical integration the displacements at these discrete points can be calculated [2].

### 4 Experiment

All experiments are performed using a system of two shaking tables to excite a 2 meters long wooden beam, Fig. 1. The 3D non-contact optical displacement and deformation measurement system is used for data management and post-processing.

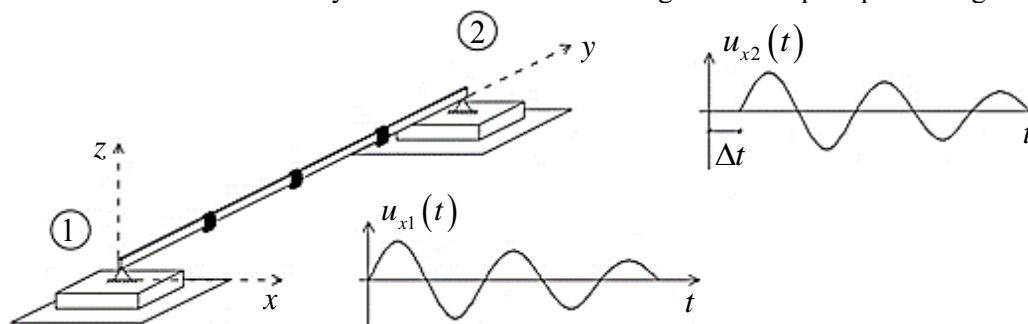


Figure1: Implementation of the experiment

### 5 Conclusion

Since theoretically based procedures for calculating dynamic response of structures subject to multi-support excitation already exist in literature [1, 2], the goal of this research has been to determine the extent to which the measured results coincide with the ones obtained using these procedures. Specifically, the dynamic response of the simply supported beam to both synchronous and asynchronous harmonic excitation as well as uniform and non-uniform earthquake excitation has been analysed.

### References

- [1] Chopra, A. K., 1995. *Dynamics of structures: theory and applications to earthquake engineering*. Prentice Hall, Englewood Cliffs (New Jersey)
- [2] Fajfar, P., 1984. *Dinamika gradbenih konstrukcij*. Univerza v Ljubljani, FAGG, Ljubljana

# Fuel cost analysis in new ship propulsion trends

**Darko Glujić**

*Faculty of Maritime Studies Rijeka*

E-mail: [darko@db-informatika.eu](mailto:darko@db-informatika.eu)

The purpose of this research is to draw conclusions on the cost-effectiveness of using natural gas as a fuel on board with dual fuel diesel-powered propulsion, both from the aspect of the fuel cheaper than the classic fuel, as well as from the ecological aspect.

Shipbuilding has always been a business where profit is in the first place. In the last few years there have been several rebounds of energy prices that have had a significant effect on both the freight rates and the volume of freight transported. To reduce the dependence on fuel price jumps, some of the ship owners decided to install dual fuel engines that could be powered by classic heavy fuel oil but also by natural gas, whose price also fluctuated, but in a closer limits. In this way, these shipping companies received alternative fuel whose price does not necessarily increase with the price of liquid fuel, and whose price in the past has not changed as much as the price of liquid fuel. This gives them the opportunity to be more competitive in certain situations, and they can plan better the company's future in aspect of the multiple choice of fuel options.

The second aspect, the ecological one, is also of utmost importance. With the enforcement of Annex VI to the Marpol Convention permitted quantities of harmful gases in the exhaust are drastically reduced. Today, new build ships must meet NO<sub>x</sub> emissions in an amount of less than 3.4 g / kWh, and will have to have less than 0.5% sulfur in fuel by 2020. [1] According to engine manufacturers, using natural gas as a fuel ship automatically meets these requirements without the need for additional specialized exhaust gas purification equipment, which is expensive to install and consumes additional resources.

One of the largest ship engine manufacturers Wärtsilä has completely abolished the production of large two-stroke diesel engines and is fully devoted to the production of four-stroke mid-range engines, focusing in particular on the development of "dual fuel" technology. For this reason, the Wärtsilä 6L46DF engine is selected from their pallet as an engine to calculate fuel costs and compare costs with different types of fuel. Behind this label is a six-cylinder engine, which develops 1145 kW of power per cylinder.

The observed engine is used to power the electric power generator, and will work most of the time at the optimum load for which it is designed. For a specific engine the optimum load is 85%, and the fuel cost for that load (according to the fuel consumption data provided by the manufacturer) is as it follows in the table (provided that 85% of the load means that the engine gives 85% of the power).

Table 1 – Fuel cost for 85% load

Period	Cost of LNG+pilot fuel \$	Cost of IFO380 \$	Cost difference
Hour	246,77	343,94	97,17
Day	5.922,48	8.254,46	2.331,97
Month	177.674,45	247.633,67	69.959,22
Year	1.954.418,90	2.723.970,32	769.551,41
5 years	9.772.094,51	13.619.851,58	3.847.757,07
10 years	19.544.189,02	27.239.703,16	7.695.514,14
15 years	29.316.283,52	40.859.554,73	11.543.271,21
20 years	39.088.378,03	54.479.406,31	15.391.028,28

The amount of exhaust gas produced for the consumption at 100% load will be calculated, as the maximum amount of exhaust gas that the engine will produce. If the engine is running at a lower load, there will be less fuel consumption, and thus the amount of exhaust gas will be lower.

The results are as it follows:

Table 2 – Comparative table of exhaust gases using liquid and gaseous fuel

Combustion product	Volume ( $m_n^3/kg_g$ ) liquid fuel	Volume ( $m_n^3/kg_g$ ) gaseous fuel	% of reduction
$V_{CO_2}$	1,47	1,226	17
$V_{H_2O}$	1,27	2,342	-84
$V_{SO_2}$	0,02	0	100
$V_{O_2}$	1,69	1,918	-13
$V_{N_2}$	14,38	16,232	-13
$V_{NOx}$	14,614	1,6966	88

The research has fully endorsed the working hypothesis. With current natural gas prices, savings in fuel costs is measured in hundreds of thousands of US dollars per engine, and one ship will most likely have several engines.

The amount of regulated exhaust gases is, as expected, several times smaller than the amount of liquid fuel exhaust gases. The very fact that a ship powered by natural gas automatically meets the Marpol Anex VI standards and does not require the installation of additional exhaust gas purification equipment brings additional savings. This savings have not been taken into account in the budget, but it is clear that it would be significant and even more emphasized the benefits of propelling using natural gas.

## References

- [1] <http://www.imo.org/en/OurWork/environment/pollutionprevention/airpollution/pages/air-pollution.aspx>

# Modelling, optimization and application of piezoelectric vibration energy harvesting devices

P. Gljušćić<sup>1, \*</sup> S. Zelenika<sup>1</sup>

<sup>1</sup> University of Rijeka, Faculty of Engineering & Centre for Micro- and Nanosciences and Technologies, Vukovarska 58, 51000 Rijeka, Croatia  
 E-mail: [pgljuscic@riteh.hr](mailto:pgljuscic@riteh.hr), [sasa.zelenika@riteh.hr](mailto:sasa.zelenika@riteh.hr)

## 1. Introduction

Energy harvesting is the process of collecting low-level ambient energy and converting it into electrical energy used to power miniaturised autonomous devices, sensor networks, wearable electronics or Internet-of-Things components. The considered ambient energy sources comprise solar/light energy, waste heat, kinetic energy and radio-frequency. Especially interesting is the use of the pervasive kinetic energy that can be converted into electrical energy via the electromagnetic effect, the electrostatic principle or the electro-mechanical piezoelectric effect. The latter proves to be advantageous due to design simplicity, miniaturization and integration potential and high energy density [1].

This work focuses on analysing the possibility to use vibration energy, converted via the piezoelectric effect, as a viable power source. Devices used in this frame are generally based on bimorph piezoelectric cantilevers (Fig. 1). The main goal in designing such devices is achieving maximum powers for the given excitation and volume constrains.

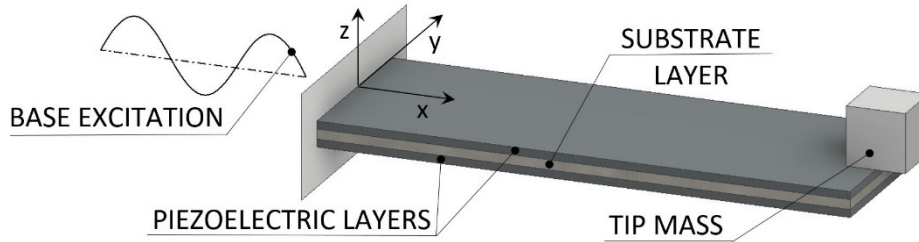


Fig. 1. Typical piezoelectric harvesting device

## 2. Coupled Electromechanical Analysis

The power output of the piezoelectric device is the highest when the harvester operates at its first eigenfrequency. Since, due to electromechanical piezoelectric coupling, the generation of electric charge in the piezo layers affects the mechanical response of the device, its behaviour must be modelled by employing the rather complex recently developed and validated “coupled modal electromechanical distributed parameter model” (CMEDM) [2]. The amplitude  $\alpha_s$  of the output voltage of the harvester is thus:

$$\alpha_s(\omega) = \frac{\sum_{r=1}^{\infty} \frac{j\omega\kappa_r\sigma_r}{\omega_r^2 - \omega^2 + j2\zeta_r\omega_r\omega}}{\frac{1}{R_l} + j\omega\frac{C_p}{2} + \sum_{r=1}^{\infty} \frac{j\omega\kappa_r\chi_r^S}{\omega_r^2 - \omega^2 + j2\zeta_r\omega_r\omega}} e^{j\omega t} \quad (1)$$

where  $\omega$  is the excitation frequency close to the eigenfrequency  $\omega_r$ ,  $\kappa_r$  is the forward coupling term,  $\sigma_r$  is excitation's translational component,  $\zeta_r$  is mechanical damping,  $R_l$  is

\* Corresponding author

the external load,  $C_p$  is piezo's capacitance and  $\chi_r^s$  is the modal coupling term. CMEDM is used next as a benchmark to verify and tune the finite element (FE) numerical model that will allow considering also different harvester geometrical and material configurations, thus simplifying the design process. The regular bimorph of Fig. 1 is thus considered in a configuration without and the one with the tip mass. In the numerical model, proper consideration of harvester's fixture and its excitation has to be imposed [3]. Modal analysis is hence performed to find the mechanical eigenfrequency, followed by the coupled harmonic analysis that allows determining the dynamic response in its vicinity. In the latter case, the consideration of electromechanical coupling is necessary again. This is achieved by connecting the nodes of the piezo layers' finite elements to the ends of a constant-resistance capacitor, having 0 V as the boundary condition on one of its ends.

### 3. Results and Discussion

The comparison of the CMEDM and the FE results, in terms of voltage outputs around the first eigenfrequency of the considered harvesters' configurations, is shown in Fig. 2.

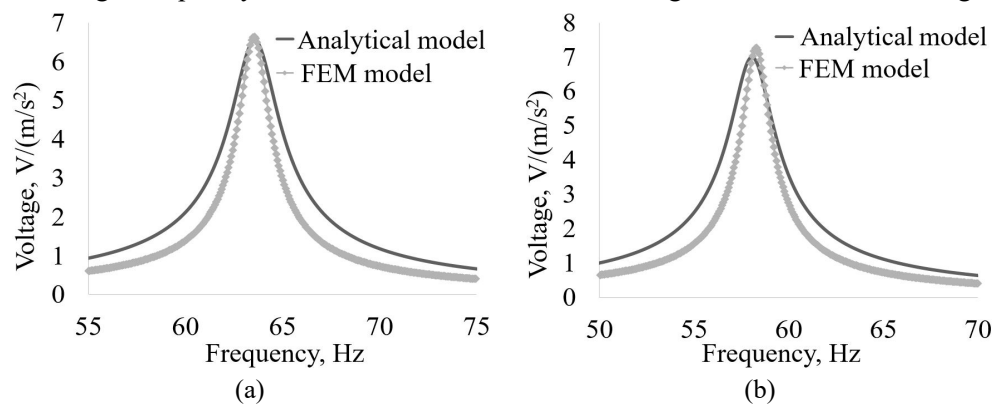


Fig. 2. Comparison of CMEDM and FE results for the harvester w/o (a) and with (b) the tip mass

It can thus be seen that in both cases the FE model allows obtaining results that closely match those obtained via CMEDM. In fact, the FE obtained eigenfrequencies match the CMEDM ones within 0.1 %. In terms of the maximal voltages the FE results are, however, higher by up to 5.5 % than those calculated via the CMEDM approach. This could imply the need for a more detailed tuning of the damping ratios of the FE model.

The given overview of the potentials of energy harvesting principles and of the modelling approaches to be applied to piezoelectric vibration harvesters is thus successfully illustrated. In the prosecution of the work, the developed FE model, extended also to coupled nonlinear transient analyses, will be applied to advanced harvesters' designs aimed at excitations varying in time or multiple excitation sources. This should allow optimising the performances of this class of devices and thus eventually employing it in innovative applications such as e.g. wearable devices for telemedicine.

### References

- [1] Blažević, D., 2014. Analysis of mechanical aspects in the design of vibration energy harvesters. D. Sc. Thesis, University of Rijeka – Faculty of Engineering.
- [2] Erturk, A. and Inman, D. J., 2009. *Smart Mater & Struct*, 18(2), 025009.
- [3] Benasciutti, D. et al., 2010. *Microsys Technol*, 16(5), pp. 657-668.

# Community detection for software-systems in evolution

**Sanja Grbac Babić, Tihana Galinac Grbac**

*Faculty of Engineering University of Rijeka, Croatia*  
*E-mail: [sgrbac@politehnika-pula.hr](mailto:sgrbac@politehnika-pula.hr), [tihana.galinac@riteh.hr](mailto:tihana.galinac@riteh.hr)*

## 1 Introduction

In recent years the Network theory has been widely used for analysing different types of networks. Considering software-system as a network, where the nodes are classes, objects or functions, and the edges are dependencies between them, the same theory can be applied for the software-systems. In this research, we have concentrated our analyses on determining community structure of network, which has not been already enough explored for the software-systems. In our work, we have analysed ten versions of a software-system in evolution. We put in exam object-oriented system Java development tool (JDT) as an evolving open-source software-system using his graph representation. The graphs where obtained in the previous work [1].

## 2 Community detection

We already know that many real-world networks exhibit division into subgraphs or communities, and the same behaviour has been observed for the software networks. The community structure approach assumes that the network divides naturally into subgraphs, and the research problem is to determine those subgraphs [2]. Every community is a locally dense connected subgraph of a network, where all nodes of a community must be reached through other nodes of the same community [3]. The presence of those structural modules indicates a deeper organizing structure of a software-system. Previous studies have shown that the application of community detection algorithms in software-systems is necessary to investigate the structure of the software. But, till now network community structure has not been completely explored, and we still have unsolved problems [4, 5]. For describing community structure of network or graph, a statistical metric is defined, called modularity. Modularity is a metric which measures the power of division of a network into communities. Networks with high modularity have dense connections between the nodes within modules but sparse connections between nodes in different modules.

## 3 Results

With Gephi's<sup>1</sup> modularity statistic, we have find communities in our graphs. Every node in the network gets assigned a module class. In this way, we can see the division of nodes into communities and the total number of communities in the network. Table 1 shows the number of nodes (N) and number of edges (E) for every version (V) of software-system, together with the corresponding number of communities (C).

<sup>1</sup> <https://gephi.org/>

Tab. 1. Size of software-system throw the evolution

V	1.0	2.0	3.0	3.1	3.2	3.3	3.4	3.5	3.6	3.7
N	803	1429	2463	2787	3305	3460	3614	3736	3780	3808
E	2605	5871	11817	13752	16482	17568	18834	19550	19879	19987
C	20	16	43	38	94	105	69	51	79	77

Due to the lack of space we only show the distribution and sizes of the communities of the version 1.0, in Fig. 1 which, indicates the presence of one huge community which includes more than a half of the nodes and some smaller but significant communities. But all the other nodes are distributed in small communities. The same behaviour has been demonstrated for all other versions of the analysed software-system.

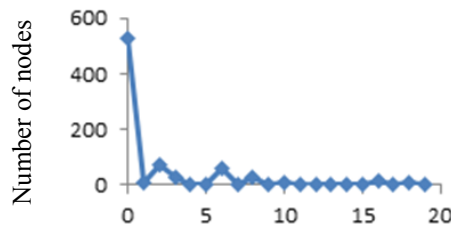


Figure 1: Distributions and sizes of communities of the version 1.0

#### 4 Conclusion

Analysing community structure properties of a software-system has showed that the examined software-systems reveal a significant community structure which confirms the presence of organized structure. Studying the structure of the system and its evolution in time can be applied for predicting future trend, reliability, maintainability, defect prediction and other software characteristics. In the future, we will expand our analyses on new versions of these open-source software systems, and we will also consider other software systems. The analyses should also be extended to other graphs and community metrics.

#### References

- [1] Petrić, J. and Galinac Grbac, T., 2014. *Software structure evolution and relation to system defectiveness*, EASE '14 Proceedings of the 18th International Conference on Evaluation and Assessment in Software Engineering, London.
- [2] Newman, M. E., 2006. *Modularity and community structure in networks*, Proceedings of the national academy of sciences, 103(23), 8577-8582.AS.
- [3] Barabási, A. L., 2016. *Network science*, Cambridge university press.
- [4] Šubelj, L. and Bajec, M., 2011. *Community structure of complex software systems: Analysis and applications*, Physica A 390 (2011) 2968–2975.
- [5] Qu, Y., Guan, X., Zheng, Q., Liu, T., Wang, L., Hou, Y., & Yang, Z., 2015. *Exploring community structure of software Call Graph and its applications in class cohesion measurement*, Journal of Systems and Software, 108, 193-210.

# Finite element analysis of a linear elastic micropolar continuum: developement of membrane elements with linked interpolation

Sara Grbčić<sup>1\*</sup>, Gordan Jelenić<sup>2</sup>

<sup>1</sup>*Faculty of Civil Engineering, University of Rijeka,  
Sorbone Universités, Université de Technologie de Compiègne*  
E-mail: [sara.grbcic@uniri.hr](mailto:sara.grbcic@uniri.hr)

<sup>2</sup>*Faculty of Civil Engineering, University of Rijeka*  
E-mail: [gordan.jelenic@uniri.hr](mailto:gordan.jelenic@uniri.hr)

## 1 Introduction

In the attempt of finding an unified continuum theory various alternative continuum theories are developed. One of them is the micropolar (Cosserat) continuum theory where, unlike the classical (Cauchy) continuum theory, the interaction between two particles is described by means of the force and moment stress vector fields [1]. As a consequence, we obtain an additional couple-stress tensor  $\boldsymbol{\mu}(\boldsymbol{x})$  as well as an completely independent microrotation field  $\boldsymbol{\varphi}(\boldsymbol{x})$ . With this assumption particles become orientable and we bring length scale into continuum theories. Due to the asymmetry of the stress and strain tensors, many new problems can be modelled. In the framework of the finite element method, in this work we present the use of linked interpolation in the design of a micropolar continuum for elastic behaviour in two dimensions where the displacement interpolation is linked not only to element nodal displacements, but also to nodal microrotations.

## 2 Micropolar continuum model

Let us analyse the body  $B$  of volume  $V$  and surface  $S$  in the deformed state under the influence of external actions consisting of distributed volume loads  $\boldsymbol{p}_v, \boldsymbol{m}_v$  and distributed surface loads  $\boldsymbol{p}_s, \boldsymbol{m}_s$ , where  $\boldsymbol{p}_v$  is a specific body force,  $\boldsymbol{m}_v$  a specific body moment,  $\boldsymbol{p}_s$  a specific surface force and  $\boldsymbol{m}_s$  a specific surface moment. By analysing the equilibrium in the deformed state we obtain the following equations:

$$\boldsymbol{\sigma}\nabla + \boldsymbol{p}_v = \mathbf{0}, \quad \boldsymbol{\mu}\nabla + \boldsymbol{a} + \boldsymbol{m}_v = \mathbf{0}, \quad (1)$$

together with the boundary conditions  $\boldsymbol{\sigma}\boldsymbol{n} = \boldsymbol{p}_s, \boldsymbol{\mu}\boldsymbol{n} = \boldsymbol{m}_s$ , where  $\boldsymbol{a}$  is an axial vector of the double skew-symmetric part of the stress tensor, i.e.  $\boldsymbol{a} = \text{axial}(2\boldsymbol{\sigma}_a)$ . By analysing geometry of the deformation process we derive the following kinematic equations:

$$\epsilon_{ij} = u_{i,j} + \epsilon_{kij}\varphi_k \quad \text{and} \quad \kappa_{ij} = \varphi_{i,j} \quad i, j, k = 1, 2, 3, \quad (2)$$

where  $\epsilon_{kij}$  is the permutation tensor,  $u_i$  is the displacement field and  $\kappa_{ij}$  is the curvature tensor. The relationship between the stress tensors  $\boldsymbol{\sigma}, \boldsymbol{\mu}$  and deformation tensors  $\boldsymbol{\epsilon}, \boldsymbol{\kappa}$  is described via six independent material constants  $\alpha, \beta, \gamma, \lambda, \mu, \nu$ , as follows:

\* Corresponding author

$$\begin{aligned}\sigma_{ij} &= \lambda \epsilon_{pp} \delta_{ij} + (\mu + \nu) \epsilon_{ij} + (\mu - \nu) \epsilon_{ji}, \\ \mu_{ij} &= \lambda \kappa_{pp} \delta_{ij} + (\alpha + \beta) \kappa_{ij} + (\alpha - \beta) \kappa_{ji},\end{aligned}\quad (3)$$

where  $\delta_{ij}$  represents the Kronecker delta.

### 3 Membrane finite elements with linked interpolation

In the framework of the finite element method, the so-called linked interpolation is derived from the exact solution of differential equations describing the Timoshenko beam subjected to uniformly distributed load. It is shown in [2] that the exact solution for the displacement field may be written in an alternative way including the contributions of the nodal rotations. One of the characteristic of such an interpolation is that the polynomial of the displacement field is one order higher than the polynomial of the rotations. The general form of the linked interpolation for arbitrary nodal points in 1D defined in [2] is equal to

$$u = \sum_{i=1}^n I_i u_i - \frac{L}{n} \prod_{j=1}^n N_j \sum_{i=1}^n (-1)^{i-1} \binom{n-1}{i-1} \varphi_i \quad (4)$$

where  $L$  is the beam length,  $n$  is the number of nodes,  $\varphi_i$  and  $u_i$  are the rotations and displacements at the  $i$ -th element node,  $I_i$  are the standard Lagrange polynomials of order  $n - 1$  and  $N_j = \frac{x}{L}$  for  $j = 1$  and  $N_j = 1 - \frac{n-1}{j-1} \frac{x}{L}$  otherwise. The solution for rotations is equal to  $\varphi = \sum_{i=1}^n I_i \varphi_i$ . Here, we generalize the form (4) to 2D and apply it to the micropolar continuum. It is important to note that, in contrast to beams, the generalized result does not follow from the solution of the differential equations of the Cosserat continuum, i.e. it is not exact. First we apply the result given in (4) at the element vertices and then we average the edge results by multiplying it with coefficients depending on arbitrary point position in order to describe the interior of the domain. Starting from the triangular element with three nodes we obtain the following generalised form of the displacement field interpolation:

$$\begin{Bmatrix} u \\ v \end{Bmatrix} = \sum_{i=1}^3 I_i \begin{Bmatrix} u_i \\ v_i \end{Bmatrix} + \frac{1}{2} \sum_{i=1}^3 (\varphi_j - \varphi_k) I_j I_k \begin{Bmatrix} b_i \\ a_i \end{Bmatrix}, \quad (5)$$

where  $i, j, k = 1, 2, 3$  denote cyclic permutation indices and  $a_i, b_i$  side-length projections along the coordinate axes.

### 4 Conclusion

Triangular and quadrilateral finite elements of different order with the corresponding linked interpolation show improved behaviour and higher accuracy comparing to elements with standard Lagrange interpolation. In order to pass the patch test, elements with even linked interpolation functions are defined using the Petrov – Galerkin finite element method, where the virtual displacements are interpolated conventionally, using Lagrange interpolation functions, and the unknown displacements interpolation is enhanced using the linked interpolation.

### References

- [1] Nowacki, W., *Theory of micropolar elasticity*, Springer-Verlag, Vienna, 1972.
- [2] Jelenić, G. and Papa E., *Exact solution of 3D Timoshenko beam problem using linked interpolation of arbitrary order*, Archive of Applied Mechanics, Vol. 81, pp. 171-183, 2009.

# Application of "Internet of things" in logistics processes

Mladen Jardas<sup>1</sup>, Paola Badurina Tomić<sup>2</sup>, Katarina Ivanić<sup>3</sup>

<sup>1</sup>*Faculty of Maritime Studies, University of Rijeka*  
E-mail: [mjardas@pfri.hr](mailto:mjardas@pfri.hr)

<sup>2</sup>*Faculty of Maritime Studies, University of Rijeka*  
E-mail: [paola.badurina@gmail.com](mailto:paola.badurina@gmail.com)

<sup>3</sup>*Faculty of Maritime Studies, University of Rijeka*  
E-mail: [kathrin.nic@hotmail.com](mailto:kathrin.nic@hotmail.com)

## 1 Introduction

Nowadays the development of all industries is based on the efficient use of information-communication technologies which represent an extremely important factor for the sustainable development of any economic branch. The application of global ICT strategy becomes necessary in all human activities [1] Its key segment is wireless communication which application is more and more present and appears as a result of continuous technological development. One of the elements of ICT strategy is sensor technology that is getting cheaper, wireless internet is getting faster and more accessible, and data processing is growing. For these reasons, the concept of "Internet of things" the so called "IoT" has been developed. This concept is an indispensable part of a larger concept - the "Internet of everything" - "IoE" which implies the networking not only of things but of people, processes, and data in a single network. [2] IoT is becoming increasingly applied in human everyday life (households, smart cities, ports, etc.) as well as in business and logistic activities. Therefore, the concept of "Internet of things" is defined as a connection of different physical objects (devices) over the Internet. [3] The term IoT includes devices connected to the Internet and their basic task is to collect and process data. These devices require the usage of information technologies that will enable the development of such smart devices that will work on the principle of data processing. The use of such devices is aimed at facilitating everyday life. It is important to point out that there is no universal application of the IoT concept in enterprises but it depends on the needs of distribution companies and changes in areas that company wants to change or upgrade. Depending on the desired changes various software solutions are created that collect data through sensors. Without Cloud and Big Data Technologies it wouldn't be possible to track data generated

by IoT. Thanks to the Cloud technology, companies have reduced their investments in computer equipment in order to store a large amount of data, and invest more in data storage on the Cloud Space. [4] The main goal of this paper is to analyze the effect and importance of the IoT technology on the distribution systems and logistics activities. The analysis also includes the impact of smart devices on physical distribution and business automation. Although the IoT technology involves the connection of devices, the interaction of people and data; when we talk about its impact on business it is referred to in the context of connecting (IoE) everything. Within this paper a concept of smart supply chain has been analyzed in which problems are detected on time, where the need of inventory replenishment arises and activities are monitored from the beginning to the end of the supply chain.

## **2 Internet of things and logistics**

Today, the transport of the goods, international, national or regional, has numerous challenges, such as continuous monitoring, analysis and optimization of the process at each step in the supply chain. Although, there are currently many devices in the transport market for the tracking of shipments, they are not connected to the Cloud and the information is not shared on time. Participants in the transportation process have difficulties to track and monitor shipments. Continuous monitoring that enables high transparency of the shipment delivery is possible and facilitated with the use of IoT technology in the logistics activities. By establishing the IoT and GPS system during the distribution on the Cloud, it is possible to track the location of each product and to see the physical characteristics of the shipment. For example, we can take smart containers that via IoT intelligent sensors exchange information with people about the current location, timely delivery, reporting of goods in the container, damage, etc. [5] Therefore, many logistics operators use the new sensor technology within the IoT concept to have constant insight into relevant data which help them to make right decisions easier. IoT sensors become more and more accessible in the transport of dangerous and temperature sensitive goods. Except for application in logistics, IoT finds a wide application in solving transport problems, such as traffic congestion, road safety, environmental protection, efficient transport of people and goods, etc. Within the supply chain, it is necessary to mention the use of IoT in warehouse processes. The advantages of using IoT in warehouses are the optimal use of warehouse, workforce and equipment components. The advantage of using IoT in warehouses is to prevent and eliminate unwanted events such as work accidents on forklifts.

## **3 Conclusion**

Based on the research, it is concluded that IoT concept greatly facilitates business in every step of distribution, but there is the question about security and protection, not just of related devices but also the amount of data which are generated in this way. Safety and protection are future challenges of this concept and represent very interesting topics for further research.

## References

- [1] Gubbi, J., Buyya, R. , Marusic, S. and Palaniswami, M., 2013. “Internet of Things (IoT): a vision, architectural elements, and future directions”, *Future Generation Computer Systems*, Vol. 29 No. 7, pp. 1645-1660
- [2] Lopez Research 2013., “An introduction to the Internet of Things (IoT)”, available at: [www.cisco.com/web/solutions/trends/iot/introduction\\_to\\_IoT\\_november.pdf](http://www.cisco.com/web/solutions/trends/iot/introduction_to_IoT_november.pdf) (06.09.2017.)
- [3] Miorandi, D. , Sicari, S. , Pellegrini, F.D. and Chlamtac, I., 2012., “Internet of things: vision, applications and research challenges”, *Ad Hoc Networks*, Vol. 10 No. 7, pp. 1497-1516, available at: <https://irinsubria.uninsubria.it/retrieve/handle/11383/1762288/2389/IOT.pdf> (01.09.2017.)
- [4] Ashton, K.,2009. “That ‘Internet of Things’ Thing”, *RFID Journal*, available at: [www.rfidjournal.com/articles/view?4986](http://www.rfidjournal.com/articles/view?4986) (04.09.2017.)
- [5] Port of Hamburg Case Study, 2016. *The Internet of Things in Transportation*, 2016.

# Numerical Analysis of the Influence of Natural Convection on Melting and Solidification of Paraffin

Mateo Kirinčić\*, Anica Trp

*Faculty of Engineering, University of Rijeka*

E-mail: [mateo.kirincic@riteh.hr](mailto:mateo.kirincic@riteh.hr)

E-mail: [anica.trp@riteh.hr](mailto:anica.trp@riteh.hr)

## 1 Introduction

Latent heat that is absorbed or released during solid-liquid phase change at constant or nearly constant temperature presents thermal potential that can be exploited for various purposes, from thermal energy storage to thermal management. Materials that undergo phase change are called phase-change materials (PCM), and one of the most commonly used PCMs is paraffin. Research of the transient 2D solid-liquid phase change [1-3] has dealt with analyzing and improving heat transfer conditions.

This research will attempt to assess the influence of natural convection on both melting and solidification of paraffin, by comparing averaged liquid fractions for these processes modeled with and without natural convection.

## 2 Mathematical model and numerical solution

Mathematical model is defined by computational domain, conservation equations, and initial and boundary conditions. Domain is a 25x75 mm rectangular enclosure, with thermally insulated horizontal walls, and vertical walls at constant temperature. In the initial moment, temperature is constant throughout the PCM, and in case of each process, equal to the temperature on one of the walls. Conservation equations are as following:

$$\frac{\partial \rho}{\partial t} + \text{div}(\rho \cdot \vec{w}) = 0 \quad (1)$$

$$\frac{\partial}{\partial t}(\rho \cdot \vec{w}) + \text{div}(\rho \cdot w_x \cdot \vec{w}) = -\frac{\partial p}{\partial x} + \rho \cdot g_x + \text{div}(\eta \cdot \text{grad } w_x) \quad (2)$$

$$\frac{\partial}{\partial t}(\rho \cdot \vec{w}) + \text{div}(\rho \cdot w_y \cdot \vec{w}) = -\frac{\partial p}{\partial y} + \rho \cdot g_y + \text{div}(\eta \cdot \text{grad } w_y) \quad (3)$$

$$\frac{\partial}{\partial t}(\rho \cdot H) + \text{div}(\rho \cdot \vec{w} \cdot H) = \text{div}(\lambda \cdot \text{grad } T) + S \quad (4)$$

\* Corresponding author

Equations (2) and (3) are omitted if a model does not include natural convection. The problem was solved using the finite volume method. For pressure and velocity coupling, the SIMPLE algorithm was used. Numerical calculations were performed in Ansys 16.2 (Geometry, Mesh, Fluent).

### 3 Results and Discussion

Values of liquid fraction for all performed analyses in a period of 600 seconds, as well as model validation, are presented in Fig. 1.

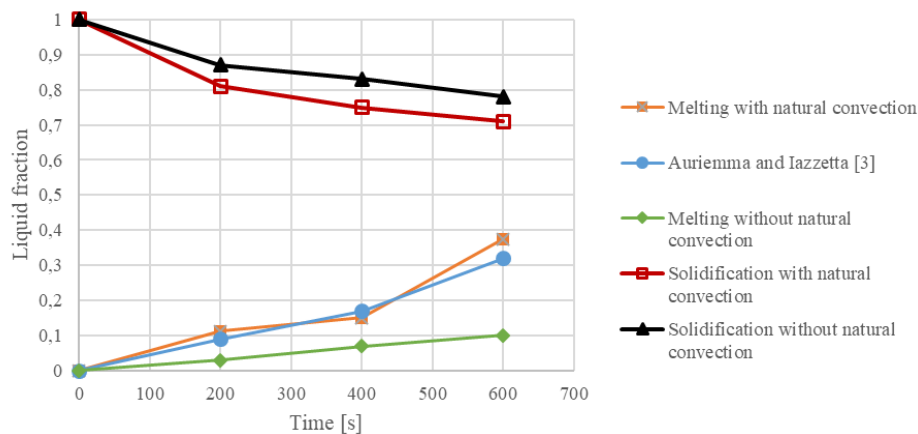


Fig. 1. Averaged values of liquid fraction for analyzed processes

It can be observed that liquid fraction for melting with natural convection is in good agreement with published results [3]. Although natural convection has effect on both melting and solidification, as time progresses, its effect on melting gets more intense.

### 4 Conclusion

Influence of natural convection on paraffin melting and solidification has been studied. By analyzing liquid fractions, it has been concluded that natural convection has significant and increasing effect on melting, and not as substantial on solidification.

### References

- [1] Muhammed S.K., Aikkara, R., Kadengal, A., 2014. Analysis and Optimisation of Melting Eate of Solids PCM for Various Shapes and Configurations, *Intl J Emerging Engineering Research and Technology*, 2(7), pp.173-183.
- [2] Arasu, A.V., Mujumdar, A.S., 2012. Numerical study on melting of paraffin wax with  $Al_2O_3$  in a square enclosure, *Intl Communications in Heat and Mass Transfer*, 39, pp.8-16.
- [3] Auriemma, M., Iazzetta, A., 2016. Numerical Analysis of Melting of Paraffin Wax with  $Al_2O_3$ , ZnO and CuO Nanoparticles in Rectangular Enclosure, *Indian J Science and Technology*, 9(3), doi: 10.17485/ijst/2016/v9i4/72601

# Laboratory analysis of evacuation spillways in water supply system of Zvir in Rijeka

Sara Kuzma<sup>1,\*</sup>, Vanja Travaš<sup>2</sup>

<sup>1</sup>*Affiliation*

E-mail: [sara.kuzma@student.uniri.hr](mailto:sara.kuzma@student.uniri.hr)

<sup>2</sup>*Affiliation*

E-mail: [vanja.travas@gradri.uniri.hr](mailto:vanja.travas@gradri.uniri.hr)

## 1. Introduction

Due to the lack of field measurements of flow and water level, a laboratory analysis of the evacuation area of Zvir waterworks in Rijeka was conducted, consisting of three overflow areas for the purpose of determining rating curves. The participating buildings were scaled to a laboratory scale and all required data was collected, a precise digital model was created and a physical model was built. A test plan has been developed to be performed on the model. The physical model is located in the experimental pool of the hydrotechnical laboratory of the Faculty of Civil Engineering in Rijeka. The conducted laboratory tests will result in the rating curves for the different opening of the gate. The efficiency of existing evacuation facilities will be tested in a time of high waters.

## 2. The digital model

### 2.1. Scaling

The Zvir source area of 80x60 meters of nature is scaled to a laboratory scale of 1:20 at 4x3 meters. The physical model must meet the geometric, kinematical and dynamic condition of similarity. To achieve geometric similarity, it was necessary to scale all the lengths, surfaces and volumes according to the following ratio:

$$L_R = \frac{L_p}{L_m}$$

where  $L_R$  is the length meter,  $L_p$  is the value of the length in nature, and  $L_m$  is the value of the length on the model. The establishment of kinematic similarity ensured similarity with kinematic sizes and preconditions for ensuring dynamic similarity.

\* Corresponding author

## 2.2. 3D scanning

From the collected data and technical drawings, the overflow area was not clearly defined and it was decided to scan the 3D area. To get a 3D cloud point a 3D Faro Focus X130 scanner with a working range of 0.6 to 130 m, a maximum deviation of +/- 2 mm, and a resolution of 70 mega pixels was used. Using the 3D cloud point, precise dimensions of the overflow, the overflow opening and the gate between the Zvir source pool and the river Rječina were determined.

## 2.3. AutoCAD model

By merging all the sketches, a digital 3D model was created in AutoCAD. The obtained model was scaled at the scale of 1:20 and the layout of the future physics in the pool of hydrotechnical laboratory was determined.

## 3. The physical model

According to the digital model, a physical model was constructed, fig. 1. Wooden plywood panels were used for the base and edges of the model, concrete cubes measuring 15x15x15 cm for the foundation of the physical model, sand, styrofoam and plastofil for the riverbed of Rječina and bottom of the pool and sponge on the water inlet into the model. The gate, overflow and overflow opening are printed using a 3D printer owned by the Rijeka Faculty of Civil Engineering, because of the desired precision 3D.



Figure 1. The physical model of the Zvir source pool and river Rječina.

## 4. Conclusion

Based on theoretical processing, the created digital and physical model, measurements and processing of results are performed to get rating curves in the Zvir pool and Rječina. The minimum and maximum flow rates of Zvir will be taken into consideration and for each case the evacuation power of each part of the overflow will be examined.

## References

- [1] Agroskin I. I., 1973. *Hidraulika*. Zagreb: Tehnička knjiga.
- [2] Rubinić J., Travaš V., Radišić M., 2017. Definiranje protočne krivulje preljeva izvora Zvir. Rijeka.

# Numerical Buckling Analysis of Thin-walled Frames with Joint Effect

Sandra Kvaternik<sup>1,\*</sup>, Goran Turkalj<sup>2</sup>, Domagoj Lanc<sup>3</sup>

<sup>1</sup>*Faculty of Engineering, University of Rijeka*  
E-mail: [sandra.kvaternik@riteh.hr](mailto:sandra.kvaternik@riteh.hr)

<sup>2</sup>*Faculty of Engineering, University of Rijeka*  
E-mail: [goran.turkalj@riteh.hr](mailto:goran.turkalj@riteh.hr)

<sup>3</sup>*Faculty of Engineering, University of Rijeka*  
E-mail: [domagoj.lanc@riteh.hr](mailto:domagoj.lanc@riteh.hr)

## 1 Introduction

Thin-walled frames are widely used in engineering practice because of their high stiffness – to – mass ratio, but structures like this, especially those composed of open thin-walled profiles, show very complex behaviour [1]. Furthermore, in fields of structural stability buckling of thin-walled frames becomes very interesting problem [2-3]. Moreover, the type of the joint at the frame connection point has as well significant influence on the overall structural behaviour [4-5]. In this work, four different joint types are investigated in order to determine frame resistance to the buckling load: mitre joint, box joint, stiffened mitre joint and box/stiffened mitre joint. Two types of beam cross sections are considered, the I-beam cross section and the channel one. An L-frame clamped on both its ends is set up according to Morell's frame [6]. Numerical analysis of the structure was undertaken using MSC. Nastran's shell model consisting of eight-noded flat elements. Material of the structure is steel and it is assumed to be homogeneous, isotropic and to obey Hooke's law.

## 2 Buckling analysis

Buckling stability analysis is carried out using Eigenvalue approach through two cases: Case 1 where the frame is clamped only on its ends and it is free to bend and twist and Case 2 in which two extra constraints are added at the joint in order to examine only warping transmission. Distributed load  $q$  [kN/m] is applied on the horizontal member on the top of the cross section flange.

The results of the first buckling mode for both Cases are presented in tables (Tab. 1 and 2.). It can be seen that frame strength and behaviour changes as the type of the joint is changed. The frame with channel section has shown better resistance to the buckling load in both cases analysed, but in the Case 2 critical buckling load is higher than it is in the Case 1. Frames with mitre joint are the least resistant to the buckling load, but those with box/stiffened mitre joint show the highest critical buckling load.

\* Corresponding author

Tab. 1. Case 1: Critical buckling load  $q_{cr}$  (kN/m) due to the joint type

Joint type	Channel section	I-section
Mitre joint	15.519	8.714
Box joint	18.866	8.887
Stiffened mitre joint	22.069	9.116
Box/stiffened mitre joint	23.328	9.134

Tab. 2. Case 2: Critical buckling load  $q_{cr}$  (kN/m) due to the joint type

Joint type	Channel section	I-section
Mitre joint	27.566	12.725
Box joint	30.228	14.647
Stiffened mitre joint	29.863	14.311
Box/stiffened mitre joint	34.112	16.795

### 3 Conclusion

A numerical buckling analysis of the L-frame with different connection structures has shown that the type of the joint can reduce or increase buckling frame resistance.

The topic of future research is buckling analysis of thin-walled frames made of composite materials.

### References

- [1] F. Mohri, S.A. Meftah, N. Damil: A large torsion beam finite element model for tapered thin-walled open cross sections beams, *Engineering Structures*, Vol. 99 (2015), pp. 132-148.
- [2] G. Turkalj, J. Brnić: Nonlinear stability analysis of thin-walled frames using UL-ESA formulation, *International Journal of Structural Stability and Dynamics*, Vol. 4, No. 1 (2004), pp. 45-67.
- [3] G. Turkalj, J. Brnić, D. Lanc: Updated Lagrangian formulation for nonlinear stability analysis of thin-walled frames with semi-rigid connections, *International Journal of Structural Stability and Dynamics*, Vol. 12, No. 3 (2012), pp 45-67.
- [4] S. Krenk, L. Damkilde: Warping of joints in I-beam assemblages, *Journal of Engineering Mechanics*, Vol. 117, No. 11 (1991), pp. 2457-2474.
- [5] P. W. Sharman: Analysis of structures with thin-walled open sections, *International Journal of Mechanical Science*, Vol. 27 (1985), pp. 665-677.
- [6] P. J. B. Morrell, J.R. Riddington, F. A. Ali, H. A. Hamid: Influence of joint detail on the flexural/torsional interaction of thin-walled structures, *Thin-Walled Structures*, Vol. 24, No. 10 (1996), pp 97-111.

# Sensitivity Studies of CFD Simulations of PTS Experiment in ROCOM Facility

Fran Ledic<sup>1</sup>, Assoc. Prof. Zoran Čarija<sup>2</sup>, Dr. Bojan Ničeno<sup>3</sup>

<sup>1</sup>*General Electric*  
E-mail: fran.ledic@gmail.com

<sup>2</sup>*University of Rijeka, Faculty of Engineering*  
E-mail: zcarija@riteh.hr

<sup>3</sup>*Paul Scherrer Institute*  
E-mail: bojan.niceno@psi.ch

## 1 Background

During nuclear reactor operation, a loss of coolant accident (LOCA) can be caused by multiple reasons such as stuck valves, ruptures or line breaks to name a few. Once a LOCA is detected, an emergency procedure of injecting colder, borated water via the emergency core cooling (ECC) system is triggered in order to ensure reactor shutdown. The injected water is much colder than the water circulating the reactor during operation (coolant water), resulting in both density and viscosity differences. The difference in properties between the injected water and coolant water can cause buoyancy driven stratifications, as well as partial mixing of the coolant. This can cause large temperature gradients to appear on the reactor pressure vessel (RPV). These temperature gradients cause high thermal stresses which can cause damage to the RPV, especially in the downcomer area where the expected gradients are of greatest magnitude. Together with high pressure from inside the reactor, this rapid temperature change and high temperature gradient can lead to pressurized thermal shock (PTS), a damaging occurrence that can lead to failure of the RPV, especially on older reactors where aging and years of exposure to neutron radiation of the RPV reduces the properties of the material.

Over the last three decades, research has determined [1] that the mixing of the water cannot be assumed as homogenous (i.e. ideal mixing), as this does not yield conservative results which could be used for safety analyses. With increased computing power, CFD is becoming a viable option for such analyses. However, to be able to trust the predictions acquired by CFD, comprehensive validation work needs to be performed. Assessment of the results is not possible in an actual reactor, which led to the creation of multiple experimental facilities, replicating the geometry of a nuclear reactor. Rossendorf coolant mixing model (ROCOM), a scaled down model of a Konvoi-type nuclear reactor is such a facility.

The main purpose of this work was to investigate the influence of different turbulent models, as well as the influence of varying initial and boundary conditions on the solution. These results can be used to stress the importance of knowing the exact parameters of the simulated event, as well as to show how dangerous misinterpreting them can be.

## 2 Our work

The experiment replicated by using CFD and Fluent 16.2 as a solver is reproducing ECC situations by injecting a higher density tracer fluid which acts as colder water. The concentration of the tracer, measured by conductivity, can be linked to both the temperature, density and boron concentration fields, described by Equation 1.

$$\theta_{x,y,z,t} = \frac{\sigma_{x,y,z,t} - \sigma_0}{\sigma_1 - \sigma_0} \cong \frac{T_{x,y,z,t} - T_0}{T_1 - T_0} \cong \frac{C_{B,x,y,z,t} - C_{B,0}}{C_{B,1} - C_{B,0}} \quad (1)$$

During simulations, special consideration was taken in analyzing the influence of boundary conditions by using different outlet definitions, initial conditions, as well as the influence of time step and the number of inner iterations within a time step. The influence of different turbulent models is shown by comparing standard k- $\epsilon$ , k- $\omega$ , k- $\omega$  SST and Reynolds Stress Model. The best-estimate case, acquired by using standard k- $\epsilon$  model, is then compared to the measurements.

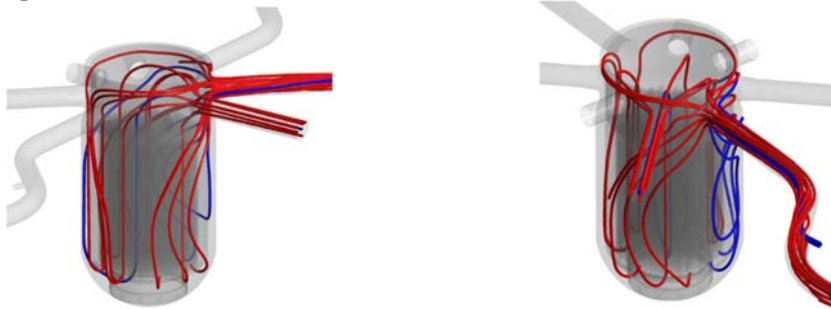


Fig. 1. Streamlines coloured by tracer - red is coolant water, blue is ECC water

## 3 Conclusion

The calculation results are a good match to the measurements, even though slight differences are evidenced. Even though the relative difference is significant at certain points, the absolute concentrations are accurately described by the simulation. The differences between sets of acquired results stress the importance of multiple factors in a CFD simulation – boundary and initial conditions, as well as mesh quality, turbulence model and time step choice. The increase of numerical and model error with increasing flow distance is also documented in the results.

The results show a tendency to overestimate the tracer concentration, which makes them conservative, as the calculated stress would be higher than actual. However, CFD results should not be taken as definite, but rather as a solid prediction. For CFD to be used as a safe tool for the nuclear industry, further investigation and evaluation of the sensitivity and different influences on mixing should be undertaken.

## References

- [1] Grundmann, U., & Rohde, U. (1994). Investigations on a boron dilution accident for a VVER-440 type reactor by the help of the code DYN3D. ANS Topical Meeting on Advances in Reactor Physics, vol. 3, (pp. 464–471). Knoxville, TN.

# Numerical analysis of a shell and tube heat exchanger

Robert Ljubek<sup>1,\*</sup>, Anica Trp<sup>2</sup>, Kristian Lenić<sup>3</sup>

*TehničkifakultetSveučilišta u Rijeci, Vukovarska 58, Rijeka, Hrvatska*  
E-mail: <sup>1</sup>[rljubek@riteh.hr](mailto:rljubek@riteh.hr), <sup>2</sup>[anica.trp@riteh.hr](mailto:anica.trp@riteh.hr), <sup>3</sup>[kristian.lenić@riteh.hr](mailto:kristian.lenić@riteh.hr)

## 1 Introduction

The basic task of any heat exchanger is to ensure transferal of heat from one medium to another. However the design and construction of heat exchangers is very complex. In this paper, a small size shell and tube water to water heat exchanger is being numerically analyzed, to present the effects of changing inlet parameters on energy and exergy efficiency. To conduct the numerical analysis of a shell and tube heat exchanger a 3D model was designed in a commercial 3D modelling software and was used as a basis to conduct a numerical analysis in a commercial CFD software. The 3D model was imported into the CFD software where it was converted to a required mesh and then divided into three domains (hot water, cold water and shell wall domain). For this particular water to water heat exchanger hot water is flowing through the inner tubes and cold water is flowing through the shell side of the heat exchanger. After defining all parameters the numerical analysis was conducted and the results for the energy and exergy efficiency will be displayed later on.

## 2 Mathematical model

The mathematical model consists of three domains, differential governing equations, initial and boundary conditions. Differential governing equations for hot and cold water domains, differential governing equations for shell wall. To simplify the numerical calculations and reduce the required computing power and resources to conduct this numerical analysis the symmetrical shape of the shell and tube heat exchanger is utilized so that the calculations are carried out only on half of the heat exchanger and then later on mirrored to get a full visualisation of results acquired during the analysis. The symmetry plain used to slice the model in half is contained on the y axis.

## 3 Results

In this chapter the results of the numerical analysis for energy and exergy efficiency will be displayed for the corresponding geometry of the shell and tube heat exchanger. The energy efficiency is calculated as a fraction of the difference between hot water inlet and outlet temperature and the difference between the inlet temperature of hot and cold water. For this analysis, the temperature of cold water is kept constant at 20°C. The results are displayed in table 1.

\*Corresponding author

Tab. 1. Energy efficiency

Case	t1'	t1''	t2''	$\eta$
1	50	24,74	34,12	0,8420
2	60	26,31	39,05	0,8423
3	70	27,93	44,13	0,8414
4	80	30,12	49,21	0,8313
5	90	34,2	54,08	0,7971

As can be seen in table 1 for the heat exchanger that was analysed in this paper the energy efficiency does not change drastically with the change of inlet temperature. Increasing the inlet temperature causes the efficiency to drop, because the difference between the inlet temperature of hot and cold water gets greater.

Tab. 2. Exergy efficiency

Case	Simulation 1				Simulation 2			
	$e_1$ (kJ/kg)	$e_2$ (kJ/kg)	$\eta$ (%)	$t_{1ulz}$	$e_1$ (kJ/kg)	$e_2$ (kJ/kg)	$\eta$ (%)	$t_{1ulz}$
1	25,518	5,406	21,187	90	25,518	5,406	21,187	90
2	18,86	3,691	19,574	80	18,86	3,691	19,574	80
3	12,933	2,269	17,543	70	12,933	2,269	17,543	70
4	8,037	1,169	14,546	60	8,037	1,169	14,546	60
5	4,2	0,3853	9,173	50	4,2	0,3853	9,173	50

From the results shown in table 2. for simulation 1 it can clearly be seen that the exergy efficiency is increasing with the increase of the inlet temperature of hot water, while the inlet temperature of cold water is kept constant, as previously mentioned. In simulation 2 we can see how the exergy efficiency behaves when we keep the temperature of the inlet hot water constant and change the inlet temperature of cold water. Increasing the inlet temperature of cold water gives this heat exchanger better exergy efficiency than the previous case with constant cold water inlet temperature.

#### 4 Conclusion

The main goal of the heat exchanger is to heat up cold water in expense of hot water. As can be seen in the results, we get better exergy efficiency if the cold water is pre-heated before entering the heat exchanger. This concept is not economically and technically viable because we are wasting energy on preheating the water that will get heated in the heat exchanger anyway, only to increase the exergy efficiency of the heat exchanger. If we have a source of waste heat at our disposal then we can utilize the increase in the heat exchanger exergy efficiency by pre-heating the cold water with the waste heat. This can be used in a combination with CHP plants and the condensers of ORC devices.

#### References

[1] Simin Wang, Jian Wen\*, YanzhongLi,: An experimental investigation of heat transfer enhancement for a shell-and-tube heat exchanger

- [2] Jian-Fei Zhang, Ya-Ling He, Wen-Quan Tao,: 3D numerical simulation on shell-and-tube heat exchangers with middle-overlapped helical baffles and continuous baffles – Part I: Numerical model and results of whole heat exchanger with middle-overlapped helical baffles
- [3] Qiuwang Wang \*, Qiuyang Chen, Guidong Chen, Min Zeng,: Numerical investigation on combined multiple shell-pass shell-and-tube heat exchanger with continuous helical baffles

My First Conference

28 September 2017

Rijeka, Croatia

## Numerical model for on-condition monitoring of condenser in coal-fired power plants

Vedran Medica-Viola<sup>1,\*</sup>, Branimir Pavković<sup>2</sup>, Vedran Mrzljak<sup>3</sup>

<sup>1</sup>*Department of Polytechnics, University of Rijeka*

*E-mail:* [vedran.medica@uniri.hr](mailto:vedran.medica@uniri.hr)

<sup>2</sup>*Department of Thermodynamics and Energy Engineering, Faculty of Engineering,  
University of Rijeka*

*E-mail:* [branimir.pavkovic@riteh.hr](mailto:branimir.pavkovic@riteh.hr)

<sup>3</sup>*Department of Thermodynamics and Energy Engineering, Faculty of Engineering,  
University of Rijeka*

*E-mail:* [vmrzljak@riteh.hr](mailto:vmrzljak@riteh.hr)

### 1. Introduction

Steam condenser is one of the essential components of the coal-fired power plant. Its performance has a major impact on the entire steam plant thermal performance [1-2].

Influence of cooling water temperature, flow rate, steam pressure and fouling on condenser performance were investigated. Steam pressure and turbine power are opposite correlated. At a lower condenser steam pressure the enthalpy drop available for the expansion in the turbine is higher, thus enabling higher turbine power and cycle efficiency. Lower condensing temperatures pressures are therefore desirable [1-2].

This paper presents a numerical model of a water cooled shell-and-tube steam condenser with single cooling water passage. The model is aimed to serve as a tool for predicting operating states in variable operating conditions. The most important steam parameter is condensing pressure, which strongly affects system efficiency. The model can be used for the condenser on-condition monitoring as well as in off-design conditions.

Steam condensation can be dropwise or filmwise, Dropwise is desirable because HTC (Heat Transfer Coefficient) is 15 – 20 times higher. The problem of determination of exact HTC on the outer surface of the tube wall, at phase changing conditions is tackled in this paper by providing a steam condenser numerical model which can easily switch between four HTC algorithms:

---

\* Corresponding author

- PADC.BE - **Physical Algorithm for Dropwise Condensation with Blowing Effect**
- PADC - **Physical Algorithm for Dropwise Condensation**
- EDC - **Empirical algorithm for Dropwise Condensation**
- PFC - **Physical algorithm for Filmwise Condensation**

## 2. Numerical model

The analyzed condenser is shell-and-tube heat exchanger. It consists of 11 700 tubes in staggered arrangement, divided in four identical almost-rectangle cross-section bundles. Active condenser area is 10 516 m<sup>2</sup>.

The model is validated using measurements on an existing condenser of the thermal power plant with the power of 210 MW. When using algorithms PADC.BE, PADC and EDC to calculate HTC, then the difference between the measured and calculated steam temperatures in the condenser at all observed condenser loads is below 4%. PFC algorithm has the highest error, up to 100%, indicating that dropwise condensation is undergoing in the analyzed condenser.

Numerical model uses iterative calculations, so a program for calculating and plotting diagrams was developed using VBA (Visual Basic for Applications).

## 3. Conclusions

The results of numerical model using each of the HTC algorithms have similar trends. Although more complicated than PADC and EDC algorithms, PADC.BE algorithm doesn't achieve higher accuracy. PADC algorithm is the latest published algorithm of those compared.

The developed numerical model can be used to easily determine the required cooling water flow rate at various condenser steam loads and cooling water inlet temperatures.

Higher cooling water flow rate demands larger cooling water pump work, causing higher operating cost. The condenser sensibility analysis, based on the developed numerical model, could be easily performed. Therefore, including cooling water pump work in the numerical model would render the model well suited for multi-objective optimization.

## References

- [1] Ahmadi, G. R., Toghraie, D.: *Energy and exergy analysis of Montazeri Steam Power Plant in Iran*, Renewable and Sustainable Energy Reviews, Vol.56 (2016) 454–463 (doi: 10.1016/j.rser.2015.11.074)
- [2] Hafdhi, F., Khir, T., Ben Yahya, A., Ben Brahim, A.: *Energetic and exergetic analysis of a steam turbine power plant in an existing phosphoric acid factory*, Energy Conversion and Management, Vol.106 (2015) 1230–1241 (doi: 10.1016/j.enconman.2015.10.044)

# A Modern Replica of Darcy Experimental Apparatus & Experimental Study of Infiltration Dynamics

Ivan Pejić<sup>1,\*</sup>, Vanja Travaš<sup>2</sup>

<sup>1</sup> Faculty of civil engineering, Radmile Matejčić 3, 51000 Rijeka, Croatia  
E-mail: [ipejic012@gmail.com](mailto:ipejic012@gmail.com)

<sup>2</sup> Faculty of civil engineering, Radmile Matejčić 3, 51000 Rijeka, Croatia  
E-mail: [vanja.travas@uniri.hr](mailto:vanja.travas@uniri.hr)

## 1 Introduction

Because of the intensification of urbanization (on the expense of “green” areas) and expansion of water impermeable surfaces, in recent times, there have been lots of negative effects on the environment e.g. the hydrogram of surface water run off became much steeper and water pollutants have much broader means of expansion. To stop these negative trends from imposing nuisance and even danger on the everyday life, engineers came up with integrated system of water drainage form urban zones. These systems contain large quantities of diverse elements like infiltration pools, retention ponds and rain gardens.

When designing a rain infiltration garden [1], besides choosing the shape and size, it is important to plan the implementation of the adequate type of soil layers and to choose appropriate types of plants to be planted in the area. The experiments conducted in the laboratory focus primarily on this aspect of rain garden’s function: how long can a soil layer contain water in order to allow the plants which are rooted in the layer to purify the water. A series of experiments were conducted with changing intensity of water influx to the system (which influences the height of the water column above the soil, that is, it regulates the pressure of the water applied to the system) and varying soil layer combinations.

To study the dynamics of water infiltration in intergranular soils, a modern replica of the Darcy experimental apparatus is constructed in Laboratory for Hydraulic Engineering at the Faculty of Civil Engineering in Rijeka. The experimental setup consist of a vertical tube equipped with probes for measurement of soil saturation..

## 2 Experimental setup

The device used in the experiments consists of one plexiglass tube and a wooden pedestal. The plexiglass tube is 2 meters high and has circular cross section with a diameter of 110 mm while the tube plate is 5 mm wide. On the tube there are 15 rectangularly shaped holes (2x4 cm) that were made with a jigsaw in the laboratory. The holes are designed to allow the implementation of water potential/content measuring sensors into the system. The pedestal is adapted to the tube and is designed in a manner

---

\* Corresponding author

that facilitates the changing of soil in the system and to allow water drainage from the device. When all the parts were ready the device was assembled in the laboratory, on the spot where the experiments would take place. When choosing a place for the device, the availability of a pump which can provide the system with running water at a height of more than 2,5 m had to be taken into consideration. It was decided that the pump of a nearby device in the laboratory would be used for providing water. The experimental apparatus is illustrated in Fig. 1 and a typical result of water content distribution along the soil column is illustrated in Fig. 2.



Fig. 1. The device with two types of soil installed

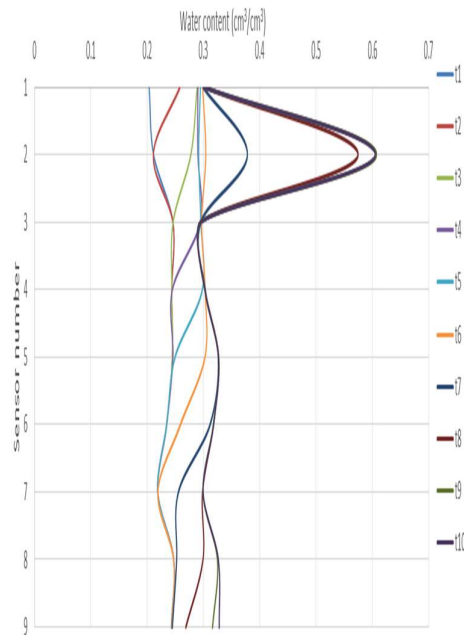


Fig. 2 Water propagation in an uniform soil column (a hole was created around sensor number 2 - one of the many problems encountered during the measurements)

## 5 Conclusion & future work

A preliminary analysis leads to a conclusion that the soil density broadly influences the results. Apart the mentioned, the constructed experimental device is found adequate to study the infiltration process that is considered. There is still plenty of space for future work. The results of the measurements will be compared to numerical infiltration models [2].

## References

- [1] Dietz, M. and Clausen, C., 2005. A field evaluation of rain garden flow and pollutant treatment. *Water air and soil pollution*, Volume 167, issue 1-4
- [2] Travaš, V., Lanča, I. 2012. Numerical model of water infiltration into unsaturated medium, *Grđevinar 10*.

# Issues in characterizing parameters influencing nanometric friction

M. Perčić<sup>1, \*</sup> and S. Zelenika<sup>1</sup>

<sup>1</sup> University of Rijeka, Faculty of Engineering & Centre for Micro- and Nanosciences and Technologies, Vukovarska 58, 51000 Rijeka, Croatia

E-mail: [mpercic@riteh.hr](mailto:mpercic@riteh.hr), [sasa.zelenika@riteh.hr](mailto:sasa.zelenika@riteh.hr)

## 1 Introduction

Friction and wear are one of the most challenging problems in many engineering and manufacturing technologies. However, while frictional phenomena on the macro to micro scales are well described and their effects can generally be efficiently compensated, the research on friction in the nanometric domain is still a matter of studies. This work is, thus, aimed at providing a contribution to the study of nanometric friction by characterising the parameters influencing its value and especially the dependence of friction on material properties, loading conditions, velocity of motion and temperature.

## 2 Experimental Methods and Results

The experimental method employed in this work is based on using the lateral force microscopy mode on a scanning probe microscope (SPM) [1]. The analysed samples, obtained by using either atomic layer or pulsed laser deposition, are: fused silica (FS), HOPG, Al<sub>2</sub>O<sub>3</sub>, TiO<sub>2</sub>, MoS<sub>2</sub>, steel, Al and nitinol. To determine the atomic concentrations and the condensed vapour thickness, prior to the measurements the samples are characterized via X-ray photoelectron spectroscopy. To carry out efficiently the experimental measurements, several issues, underlined below, need then to be considered.

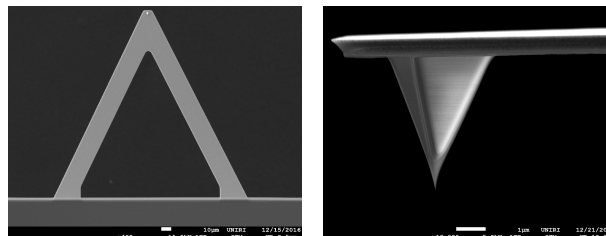


Fig. 1. SEM micrographs of the used probes

To tune the measurement conditions and quantify the obtained results, the experimental methodology involving SPM requires a precise calibration of the lateral and normal stiffness of the used probes. This calibration is performed, based on precisely measured probes' dimensions on a scanning electron microscope (SEM – Fig. 1), by using FEM and the method of parallel beam approximation, as well as by employing subsequently calibration gratings [2]. The thus obtained stiffness allow establishing that the uncertainty of the determined values is significant (up to  $\pm 15\%$ ).

The nanoscale contact between probes' tips and the samples is governed by a variety of other physical phenomena as well. To quantifying these effects, separate experimental

---

\* Corresponding author

measurements are thus performed to establish the tip wear and to characterize the samples in terms of their Young's modulus, hardness and surface adhesion.

Once this is done, the measurements on the samples can be performed. Standard design of experiments (DoE) methods such as (full) factorial design or Box-Behnken are, however, poorly suited to obtain a detailed insight into the studied multidimensional stochastic phenomenon. DoE is thus conducted in this work by defining the experimental space via sampling methods that enable the development of a meta-model. Since recent studies indicate that among these the centroidal Voronoi tessellation (CVT) [3] has several advantages, CVT is used on each of the sample materials to generate 50 points along each of the studied influencing parameters, i.e., normal force, sliding velocity and temperature.

When experimental data is available, a mathematical expression for the nanoscale friction model should be determined. Due to numerous uncertainties and the highly stochastic dependence of the coefficient of friction on the studied parameters (shown in Fig. 2 for two of the studied materials), this task proves to be very complex. Polynomial fitting of the results via the often-used multidimensional interpolation algorithms yields, however, a very poor fit with the best coefficients of determination limited to  $R^2 = 0.1$ . The obtained experimental data will thus be rather input into recently developed computational algorithms for nonlinear model representation that enable a simultaneous examination of global uncertainties and contributions of a large number of parameters.

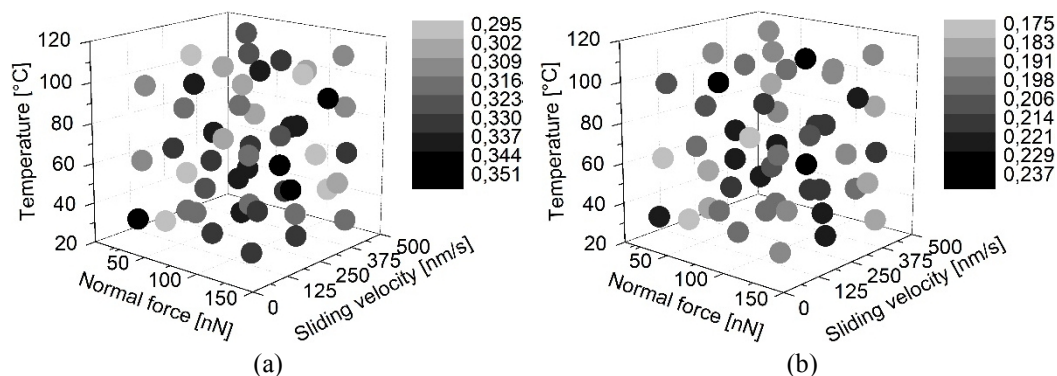


Fig. 2. Colour-coded experimentally determined values of the coefficient of nanometric friction generated via CVT vs. the influencing parameters for FS (a) and MoS<sub>2</sub> (b) samples

### 3 Conclusion and Outlook

This work provides an analysis of the numerous difficulties and issues involved in the determination of nanometric friction. The prospected results of the ongoing research will provide a significant scientific contribution to the determination of the basic principles of nanometric friction by characterising the impact of the numerous studied parameters on its value. By obtaining finally multidimensional correlation functions linking the value of nanometric friction to these variables, a possibility to extend the established friction models, so as to broaden their applicability to the nanometric range, should be provided.

### References

- [1] Bhushan, Bh. ed., 2010. *Springer Handbook of Nanotechnology*. Berlin, Heidelberg: Springer.
- [2] Perčić, M., Zelenika, S. and Kamenar, E., 2017. *Proc 17<sup>th</sup> Int EUSPEN Conf*, pp. 105–6.
- [3] Du, Q., Faber, V. and Gunzburger, M. D., 1999. *SIAM Rev*, 41(4), pp. 637–76.

# Procedure for modelling of soft tissues behaviour

**M. Franulović<sup>1</sup>, K. Marković<sup>2</sup> and S. Piličić<sup>3,\*</sup>**

<sup>1</sup> *Faculty of Engineering, University of Rijeka, Croatia*  
E-mail: [marina.franulovic@riteh.hr](mailto:marina.franulovic@riteh.hr)

<sup>2</sup> *Faculty of Engineering, University of Rijeka, Croatia*  
E-mail: [kristina.markovic@riteh.hr](mailto:kristina.markovic@riteh.hr)

<sup>3</sup> *Faculty of Engineering, University of Rijeka, Croatia*  
E-mail: [stjepan.pilicic@riteh.hr](mailto:stjepan.pilicic@riteh.hr)

Modelling the behaviour of mechanical systems and its simulation in operating conditions is an unavoidable process in optimization of their design. Modelling of material behaviour consists of describing phenomena that occur within material when subjected to the loading [1]. In order to take into account these phenomena, the appropriate constitutive material models should be used. These models are usually complex non-linear systems and, for validation, their calibration should be based on the experimental results [2].

The specific direction in biomechanical systems investigations became the modelling of behaviour of soft tissues [3], which have unique structure, and thus complex physical principles are expected to be applied for their modelling. The procedure for calibration of material model for soft tissues behaviour, in this case human cervical spine ligaments, is the focus of this investigation. Although there are several material models developed for modeling material behaviour of this biomaterial, the commonly used one [4] is based on the theory of hyperelasticity. The mechanical behaviour of soft tissues strongly depends on structural arrangement and concentration of major phases of mentioned material which are collagen fibers, elastin fibers, proteoglycans, cells and interstitial fluid phase [5]. Arrangement of these phases determines material properties of considered materials such as anisotropy, viscoelasticity and ability to undergo large deformations [6].

Human cervical spine ligaments have non-linear stress-displacement response until failure when load increases uniformly, which is recorded during tensile tests. The characteristic stress-displacement curve for investigated material is shown in Figure 1, which is adopted from [5]. It consists of three characteristic regions called toe, linear and damage (failure) region. In order to accurately simulate material behaviour, the hyperelastic material model that is suitable for numerical modeling of soft tissues has been used. To conduct the numerical procedure, a genetic algorithm shall be used. In order to define effective genetic algorithm for the parameter identification process, inverse analysis (a method of searching an unknown characteristic(s) of a sample by observing its response on a given stimulating signal) should be used.

The mechanical principles for the material behaviour of the investigated material model have been chosen for the successful inverse analysis. This allowed the definition of the objective function for the given problem and thus possibility to apply an evolutionary method, such as genetic algorithm for the optimization of identification of material parameters. The procedural steps for the efficient genetic algorithm for the parameter identification have been detailed in this investigation. The deviation between simulated and experimental materials response should be minimized, which can be

assured by choosing proper objective function and evaluated through the developed procedure. The validation of the developed procedural steps is done using data obtained through experiments, which will allow to further develop suitable genetic operators.

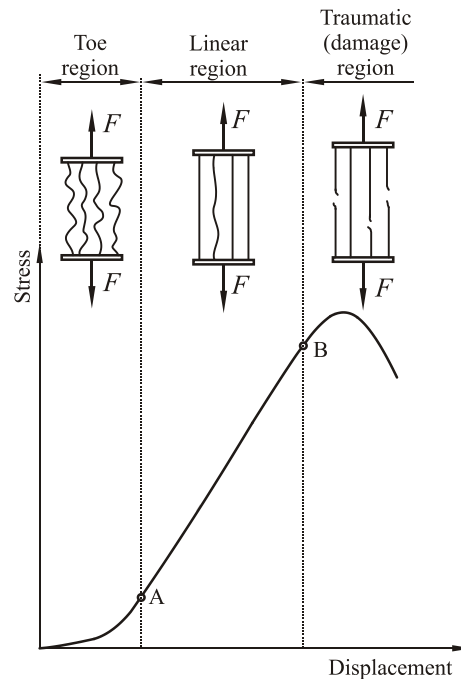


Fig. 1. Characteristic force - displacement material response, adopted from [5]

### Acknowledgements

This work has been supported by Croatian Science Foundation under the project number IP-2014-09-4982 and also by the University of Rijeka under the projects number (13.09.1.2.09) and (13.09.2.2.18).

### References

- [1] J. (Jean) Lemaître and J.-L. Chaboche, *Mechanics of solid materials*. Cambridge University Press, 1990.
- [2] L. E. Schwer, "An Overview of the PTC 60 / V&V 10 Guide for Verification and Validation in Computational Solid Mechanics," 2007.
- [3] M. Freutel, H. Schmidt, L. Dürselen, A. Ignatius, and F. Galbusera, "Finite element modeling of soft tissues: Material models, tissue interaction and challenges," *Clin. Biomech.*, vol. 29, no. 4, pp. 363–372, 2014.
- [4] J. a Weiss and J. C. Gardiner, "Computational modeling of ligament mechanics.," *Crit. Rev. Biomed. Eng.*, vol. 29, no. 3, pp. 303–371, 2001.
- [5] N. Yoganandan, S. Kumaresan, and F. A. Pintar, "Biomechanics of the cervical spine. Part 2. Cervical spine soft tissue responses and biomechanical modeling," *Clinical Biomechanics*, vol. 16, no. 1. pp. 1–27, 2001.
- [6] Y.-C. Fung, *Biomechanics Mechanical Properties of Living Tissues*. Springer, 1993.

# Modelling fibers in concrete using the XFEM methodology

Tea Rukavina<sup>1,2,\*</sup>, Adnan Ibrahimbegović<sup>2</sup>, Ivica Kožar<sup>1</sup>

<sup>1</sup>University of Rijeka, Faculty of Civil Engineering, Croatia  
E-mail: [tea.rukavina@uniri.hr](mailto:tea.rukavina@uniri.hr), [ivica.kozar@uniri.hr](mailto:ivica.kozar@uniri.hr)

<sup>2</sup>Université de Technologie de Compiègne / Sorbonne Universités, France  
E-mail: [adnan.ibrahimbegovic@utc.fr](mailto:adnan.ibrahimbegovic@utc.fr)

## 1 Introduction

Fiber reinforced concrete (FRC) is a heterogeneous material consisting of a cement matrix, aggregate and fibers. The addition of fibers leads to an increase in ductility, tensile strength, and the material's resistance to cracking. To be able to describe the material behavior and crack development, a finite element model has been developed.

## 2 Numerical model

In this work, concrete is modelled with triangle (CST) elements, and the steel fibers are modelled as truss bar elements. The material model chosen for concrete is damage, with a softening part describing the crack opening. This has been taken into account by introducing an embedded strong discontinuity which models the displacement jump. The behavior at the discontinuity is described by a traction-separation cohesive law.

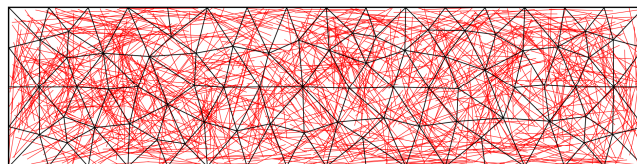


Fig. 1. Non-conforming meshes of concrete (black) and fibers (red)

The main challenge in modelling this kind of heterogeneous material is taking into account the fibers. They are randomly distributed inside the domain, and their nodes do not usually coincide with the main nodes of the concrete finite elements (see Fig. 1.). One of the possible ways to solve this problem is to use the extended finite element method (XFEM) [1], where inclusions and discontinuities are taken into account by using global enrichment functions. In general, the displacement field for an enriched element can be represented as:

$$\mathbf{u}(\mathbf{x}) = \sum_{i=1}^n N_i(\mathbf{u}_i + \phi \boldsymbol{\alpha}_i) \quad (1)$$

---

\* Corresponding author

where  $n$  is the number of nodes in the element,  $N_i$  are the shape functions in node  $i$ ,  $\mathbf{u}_i$  are the standard displacements,  $\boldsymbol{\alpha}_i$  are the enriched displacements, and  $\phi$  is the global enrichment function. In [2], there are two enrichments, one taking into account the presence of the fiber in the domain, and the other describing the debonding between the fiber and the surrounding matrix.

In [3], the XFEM methodology is used to model a standard reinforced concrete structure, but the same principle can be applied to FRC. In the elastic phase, concrete and steel have the same displacement, but when the first crack in concrete appears, the bond-slip on the interface between steel and concrete becomes active. Since the steel is stronger than the bond on the interface, the latter is the first one to fail. In other words, the fiber will be pulled out before it breaks.

#### 4 Experimental testing of bond-slip

Since the bond-slip mechanism is important for understanding the behavior of the material [4], experimental tests have been performed. Single-fiber pull-out tests have been carried out on specimens with two different embedded lengths of the fibers. The results show a steep post-peak response of the specimen with the smaller embedded length, due to less pronounced frictional dissipation, compared to the specimen with the larger embedded length.

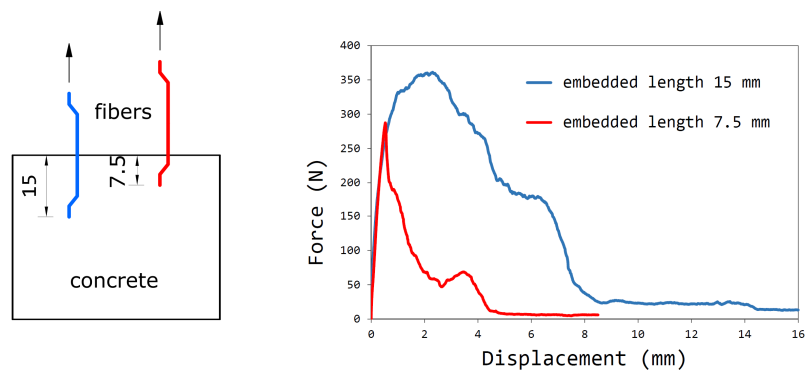


Fig. 2. Results of the single-fiber pull-out tests with different embedded lengths

#### References

- [1] Fries, T.-P. and Belytschko, T., 2010. The extended/generalized finite element method: an overview of the method and its applications. *International Journal for Numerical Methods in Engineering*, 84(3), pp. 253–304
- [2] Pike, M.G. and Oskay, C., 2015. XFEM modeling of short microfiber reinforced composites with cohesive interfaces. *Finite Elements in Analysis and Design*, 106, pp. 16–31.
- [3] Ibrahimbegovic, A. et al., 2010. Modelling of reinforced-concrete structures providing crack-spacing based on X-FEM, ED-FEM and novel operator split solution procedure. *International Journal for Numerical Methods in Engineering*, 83(4), pp. 452–481.
- [4] Dominguez, N. et al., 2005. Prediction of crack pattern distribution in reinforced concrete by coupling a strong discontinuity model of concrete cracking and a bond-slip of reinforcement model. *Engineering Computations*, 22(5/6), pp. 558–582.

# Heat Transfer Fluid Storage in the Solar Collection Loop – The Storage Volume Impact on the Work Performance of a Solar Absorption Cooling System

Fran Torbarina<sup>1,\*</sup>, Kristian Lenić<sup>2</sup>

<sup>1</sup>Faculty of engineering, University of Rijeka  
E-mail: [fran.torbarina@uniri.hr](mailto:fran.torbarina@uniri.hr)

<sup>2</sup> Faculty of engineering, University of Rijeka  
E-mail: [kristian.lenic@uniri.hr](mailto:kristian.lenic@uniri.hr)

## 1 Introduction

Due to the intermittent nature of solar energy during days and its absence during nights, special attention has to be paid to the thermal energy storage when designing a solar absorption cooling system. Such systems can improve the overall efficiency by enabling continuous operation or by extending the working hours of a cooling system [1 – 4]. The main goal of this paper is to determine how a hot water thermal energy storage volume, placed in solar loop, impacts the work performances of an absorption cooling system and to find the optimum storage volume for given solar collector area and nominal capacity of a chiller.

## 2 System description

The proposed system incorporates several main components – evacuated tube solar collectors, a hot water thermal energy storage, an absorption chiller (10 kW rated capacity), a wet cooling tower and a small capacity cold storage. Schematic representation of the system is shown in Figure 1.

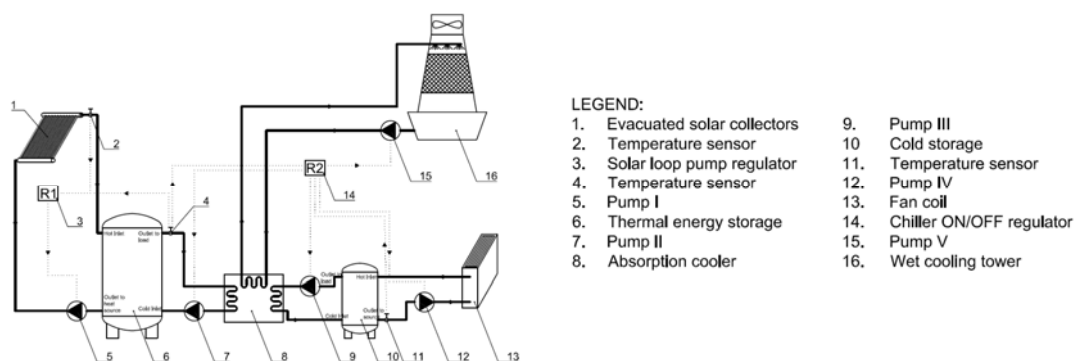


Figure 1. Schematic representation of the analysed system

\* Corresponding author

### 3 Simulation in TRNSYS

Numerical analysis has been done using TRNSYS software. Total of 20 different simulations have been performed, one for each hot water storage volume from 0.2 m<sup>3</sup> to 4.0 m<sup>3</sup> with step of 0.2 m<sup>3</sup>. The observed parameters were total working time and total energy exchanged in the evaporator of the absorption chiller.

### 4 Results

Both total working time and total cooling energy have maximum values for the hot water storage volume of 2.4 m<sup>3</sup>, Figure 2, which means that for every square meter of evacuated tube solar collectors the heat storage volume should be about 37 liters and for every 1 kW of chiller's rated capacity the heat storage volume should be 240 liters.

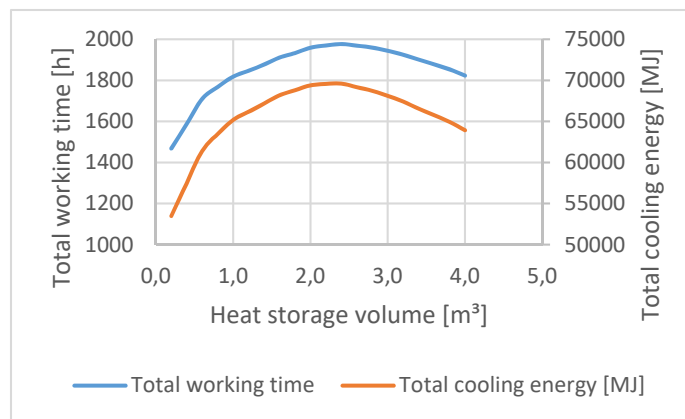


Figure 2. Graphical representation of the data obtained through the system simulation

### 5 Conclusion

The simulation showed that the heat storage with a volume of 2.4 m<sup>3</sup> in the solar loop reduces the effect of short term fluctuations in the solar radiations, stores the excess heat in the periods with high solar availabilities for the use in periods with low solar availabilities and prolongs the total working time of the proposed system.

### References

- [1] Delač, B., 2017. *Optimization of Energy Systems for Nearly Zero Energy Buildings Using Dynamic Simulations – Doctoral thesis*. Faculty of Engineering, University of Rijeka
- [2] Belmonte, J.F., Izquierdo-Barrientos, M.A., Eguia, P.A., Molina, E., Almendros-Ibaandnbspnez, J.A., 2014. PCM in the heat rejection loops of absorption chillers. A feasibility study for the residential sector in Spain. *Energy and Buildings*, 80, pp.331–351.
- [3] Helm, M., Keil, C., Hiebler, S., Mehling, H., Schweigler, C., 2009. Solar heating and cooling system with absorption chiller and low temperature latent heat storage: energetic performance and operational experience, *International Journal of Refrigeration*, 32, pp.596–606.
- [4] Agyenim, F., 2016. The use of enhanced heat transfer phase change materials (PCM) to improve the coefficient of performance (COP) of solar powered LiBr-H<sub>2</sub>O absorption cooling systems, *Renewable Energy*, 87, pp.229-239

# Rocking of a Block due to Base Movement

Miran Tuhtan\*, Gordan Jelenić

*Faculty of Civil Engineering Rijeka*

E-mail: [miran.tuhtan@gradri.uniri.hr](mailto:miran.tuhtan@gradri.uniri.hr) , [gordan.jelenic@gradri.uniri.hr](mailto:gordan.jelenic@gradri.uniri.hr)

## 1 Introduction

A solid rectangular block lying on a rigid or flexible simply-supported beam-type base is considered, in which the beam supports are subject to a prescribed uniform horizontal in-plane motion. The block can then experience three different types of motion: (a) translation together with the base, (b) rocking and overturning, (c) stable rocking without overturning.

The experiments are conducted for sinusoidal base movement with beams of varying stiffness to test how the elasticity of the beam base affects the block stability.

## 2 Experiment

The stability of aluminium block with the dimensions 3 x 3 x 15 cm, and with the mass of 339 g is tested for the sinusoidal movement with amplitudes ranging from 0.1 to 2.0 cm in 0.1 cm increments, and frequencies ranging from 1.0 to 5.0 Hz in 0.2 Hz increments on Quanser Shake Table I-40 single-axis earthquake simulator [1].

The stiff base is made by 3D printing using Full Cure Vero White 835 material [2]. A set of elastic beams of length  $L = 230$  mm, width  $B = 100$  mm, and thickness  $H = 2, 3, 4, 6, 8, \text{ or } 10$  mm are made of balsa wood with the measured modulus of elasticity of  $E = 2.29$  GPa.

## 3 Numerical calculation

The equations of motion of a block depend on the sign of the current angle of inclination  $\theta$  of the block side with respect to the vertical. Equating the sum of vertical forces and the sum of moment around the overturning point for the block on the elastic beam with the respective changes in the linear and angular momentum, and assuming a small angle  $\theta$  with no slipping and bouncing of the block with respect to the base, we get

$$\begin{bmatrix} \frac{4}{3}R & \mp \sin \alpha \\ \mp \sin \alpha & \frac{1}{R} \end{bmatrix} \begin{Bmatrix} \ddot{\theta} \\ \ddot{y} \end{Bmatrix} + \begin{bmatrix} -g \cos \alpha \mp \ddot{u} \sin \alpha & 0 \\ 0 & \frac{k}{mR} \end{bmatrix} \begin{Bmatrix} \theta \\ y \end{Bmatrix} = \begin{Bmatrix} \ddot{u} \cos \alpha \mp g \sin \alpha \\ \frac{g}{R} \end{Bmatrix} \quad (1)$$

where  $y$  is the vertical displacement of the block-beam contact point,  $R$  is a half of the planar diagonal of the block,  $\alpha$  is the angle determined by the width-height ratio of the block,  $g$  is gravitational acceleration,  $\ddot{u}$  is the prescribed base acceleration,  $k = 48EIL / (L^2 - b^2)^2$  is the base stiffness at the point of block-base contact, where  $I = BH^3 / 12$ , and  $b$  is the block width, and  $m$  is the mass of the block.

\* Corresponding author

Equation (1) is solved using Newmark's trapezoidal rule [3] with a time-step length equal to  $\Delta t = 0.0001$  s. The dissipation of the kinetic energy at the time of contact of the base and the block is taken into account using the reduction in angular velocity derived in [4]. The algorithm is coded in Python 3.6.1 using the NumPy package [5].

#### 4 Results

In both the numerical calculation and the experiment, all three different types of movement of the blocks are present, which can be seen in Fig. 1 for the beam 8 mm thick, where the shaded area represents translation, the area marked by crosses represents stable rocking, and the area marked by dashes represents overturning. The unshaded area represents the situation in which the base acceleration runs above the upper limit of the equipment (1 g). Clearly, some discrepancies between the experiment and numerical calculation can be observed. Similar behaviour is also present in the beams of different thickness as well as the rigid base.

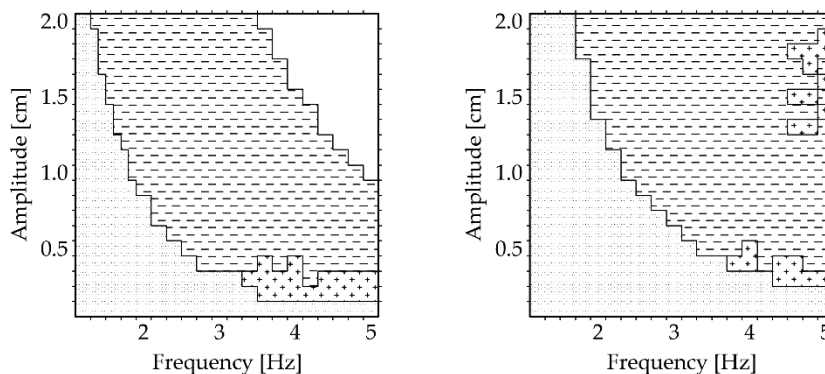


Fig 1. The results for the 8 mm thick base: a) experimental results, b) numerical results

#### 5 Conclusion

In our future work we plan to investigate why the discrepancies between the experiment and the simulation arise. We will analyse if a non-linear beam model describes the problem better, and run the experiments on more powerful shake tables thus including the cases in which the ground acceleration may exceed 1 g.

#### References

- [1] Quanser, *Shake Table I-40 Technical Specifications*, viewed 5 September 2017, [http://www.quanser.com/products/shake\\_table\\_I](http://www.quanser.com/products/shake_table_I).
- [2] Stratasys, *Vero white Full cure 835*, viewed 25 August 2016, <http://www.stratasys.com/materials/material-safety-data-sheets/polyjet/rigid-opaque-materials>.
- [3] Bathe, K.J., 1996. *Finite element procedures*. Prentice Hall, New Jersey.
- [4] Housner, G.W., 1963. The behavior of inverted pendulum structures during earthquakes. *Bulletin of the seismological society of America*, 53(2), pp.403-417.
- [5] NumPy developers, *NumPy*, viewed 5 September 2017, <http://www.numpy.org/>.

# Shear design and diagonal crack control of reinforced concrete beams

Hrvoje Vido<sup>1,\*</sup>

<sup>1</sup> University of Rijeka, Faculty of Civil Engineering  
E-mail: [hrvoje.vido@uniri.hr](mailto:hrvoje.vido@uniri.hr)

## 1 Introduction

Due to load redistribution between concrete and reinforcement in shear design of reinforced concrete beams, internal beam stress-strain state is still not simply defined. Most widely used design models include analogy with truss model and implementing nonlinear analyses to define internal state, what makes it impractical in everyday use.

Current European standards define simple truss model with free choice of compressive strut angle for shear design and no guidelines for state of diagonal cracking check. Although dimensioning is reasonably well defined, some investigations imply that overestimation of load capacity may occur, if selected lower compressive strut angle. Cracking is defined only for simple bending model and assumed to be larger on diagonally stressed beam because reinforcement coincides at different angle than principal tensile stresses. These lacks make verification difficult or even impossible to do by designer.

Goal of this research is defining simple mathematical model to improve verification of shear design and control of diagonal cracks.

## 2 Variable angle truss model with implementation of modified compression field theory

Ritter and Mörsch have noticed analogy between concrete beam and simple truss model to simplify reinforced concrete beam design [1]. Analogy consists of separately dimensioning: bending load is transferred by flanges; while shear transfer occurs in web, as shown in Figure 1. In case of bending, concrete is considered as compressive flange and reinforcement as tensile flange. Web consists of concrete compressive diagonal struts inclined from horizontal axis by angle  $\Theta$  and stirrups whose inclination  $\alpha$  may vary, but most widely used is orthogonal  $\alpha=90^\circ$ . While defined truss system is undetermined, static determinacy may be obtained by free choice of strut angle in limits  $[21.8^\circ-45^\circ]$  (defined in EN1991-1-1 2005 [2]) or by defining appropriate stress-strain state which leads to reduction of unknown parameters.

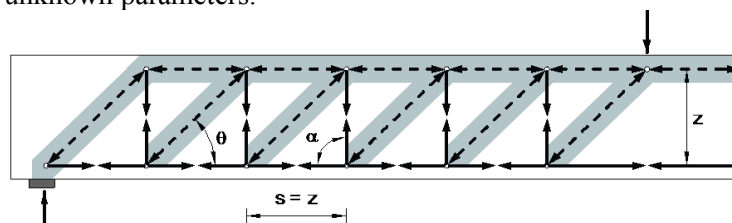


Figure 1. Modified truss analogy [1]

\* Corresponding author

One of verification procedures, defined by Canadians Mitchell and Collins is called “Modified compression field theory” [3]. Modeling includes nonlinear analysis and defines stress-strain state as function of principal principal axis angle  $\Theta$  for fixed, freely chosen tensile deformation  $\epsilon_1$ , using equilibrium, stress-strain and compatibility equations. In two beam design examples, method comparison has shown that low strut angle choice  $21.8^\circ$  overestimates design load, and it shall be avoided in practice [4].

### 3 Diagonal crack control

Crack control in reinforced concrete structures is important for appearance, water tightness and corrosion protection. Internal stress-strain state calculated by using modified compression field theory can be extended to define diagonal crack widths and spacing (Figure 2.). According to experiments, most important design parameters for crack control are already known, but after initiation of cracking, continuous stress redistribution influences variable crack widths and unpredictable angle of opening. Future research includes combination of cracking theory [3,5], and experimental analysis to define simplified model for approximation of average and characteristic crack widths and crack spacing for serviceability load state.

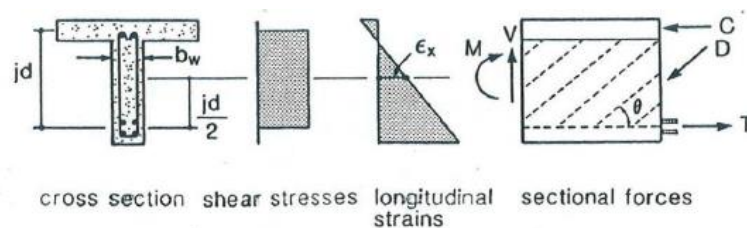


Figure 2. Stress-strain state according to modified compression field theory [3]

### 5 Conclusion

Nonlinear analysis by using modified compression field theory has confirmed that limitations of lower strut angle in variable angle truss model shall be redefined. Crack control is important mostly because of durability and appearance aspects. Simplified diagonal crack verification model, which can be implemented into Code control procedure, will be proposed after future research.

### References

- [1] Grandić D., Šećulac P., Grandić I.Š., 2015. Shear resistance of reinforced concrete beams in dependence on concrete strength in compressive struts, Tehnički vjesnik 22, vol. 4, 925-934
- [2] EN 1992-1-1: Part 1-1, 2004. General rules and rules for buildings, Eurocode 2 – Design of concrete structures, European committee for standardisation, Bruxelles
- [3] Collins, M.P., Mitchell, D., 1997. Prestressed Concrete structures, Response publications, 309-379.
- [4] Vido, H., 2014. Behavior of reinforced concrete beams subjected to shear, Master thesis, Rijeka
- [5] CEB, 1985., CEB Design Manual on Cracking and Deformations, École polytechnique fédérale de Lausanne

# Ship speed and fuel consumption: the effect of waves on ship and engine dynamics

Natalija Vitali<sup>1,\*</sup>, Jasna Prpić-Oršić<sup>2</sup>

<sup>1</sup>Faculty of Engineering, University of Rijeka  
E-mail: [natalija.vitali@riteh.hr](mailto:natalija.vitali@riteh.hr)

<sup>2</sup> Faculty of Engineering, University of Rijeka  
E-mail: [jasnapo@riteh.hr](mailto:jasnapo@riteh.hr)

## 1 Introduction

Energy efficient maritime transport has become one of the most important topics in shipping. The impact of emissions from marine transport have led to stricter regulations limiting the emissions from seagoing vessels [1]. New technologies are being implemented to both the existing fleet and the new buildings in order to satisfy the regulations and endure in the competitive market influenced by fuel prices and crisis. The technological measures for a more efficient ship include improved engine, ship hull and propeller design, use of cleaner fuels (low carbon content, renewable energy sources, LNG). Logistic measures include weather routing and fleet management. [2] Within both issues, predicting attainable speed is an important topic. Ship speed assessment influences ship route planning, expected time of arrival, fuel consumption and emissions estimations. The even more significant problem arises from the estimation of speed in rough weather conditions.

## 2 Estimation of attained speed and fuel consumption

Global shipping initiatives and efforts to make “greener” ships have led to optimization of the ships in actual environmental conditions, as opposed to the traditional methods of observing ships in calm water conditions. The estimation of ship performance is best described by observing coupled engine and ship models [3] as shown in Fig. 1.

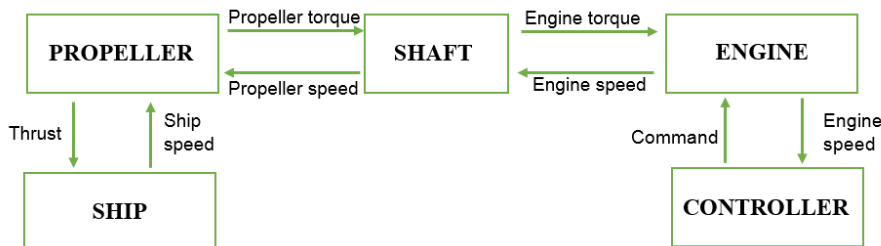


Fig. 1. Coupled model for ship and engine simulation

\* Corresponding author – Natalija Vitali

The results of the estimation of speed loss and fuel intake using the above described model are shown in Fig. 2. The analysis is done for a Handymax bulk carrier under the influence of waves of significant wave height of 7 meters. Fig. 2. illustrates the changes in ship resistance in waves along with the change in ship speed. Extra environmental resistance causes the ship to slow down. The decreased ship velocity changes the advance ratio of the propeller leading to increased torque and reduced engine speed. The controller in charge of maintaining the desired engine speed and responds to the increased resistance by introducing more fuel to the engine. This model provides us with real time estimations of ship and engine parameters in the presence of waves and represents a tool for more accurate estimations of ship performance in realistic conditions.

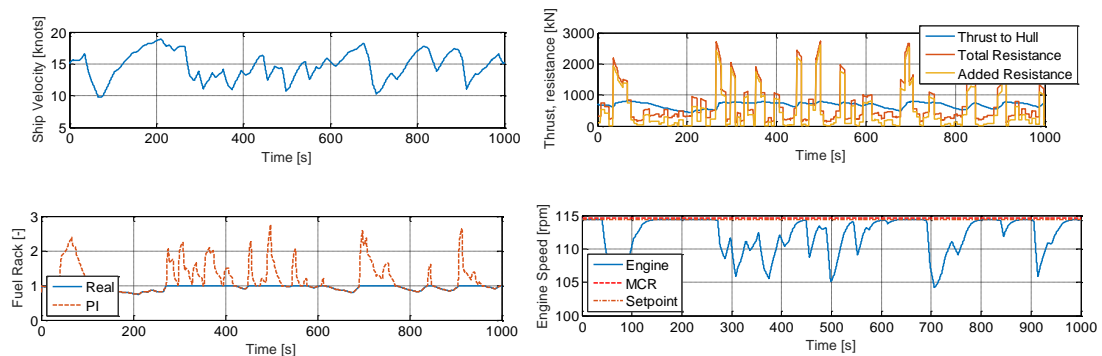


Fig. 2. Speed loss of a bulk carrier in waves

## 5 Conclusion

The presence of waves affects ship propulsion system. Ship added resistance, wake variations, propulsion losses can have a significant influence on vessel performance. Propeller performance is influenced by the changes in wake, loss of ship speed, variations in propeller revolutions as well as the ship motions. Excessive ship motions can cause propeller emergence and ventilation. This condition can lead to changes in engine performance leading to the conclusion that propeller and engine should be observed as a system in order to properly describe their interactions.

## References

- [1] MEPC, IMO, 62/5/19, Reduction of GHG emissions from ships-consideration of the Energy Efficiency Design Index for new ships (2011).
- [2] H. N. Psaraftis, 2012. Market-based measures for greenhouse gas emissions from ships: a review, *WMU Journal of Maritime Affairs* 11 (2) pp. 211-232.
- [3] Taskar, B., Yum, K.K., Pedersen, E., Steen, S., 2015. Dynamics of a marine propulsion system with a diesel engine and a propeller subject to waves. In: *Proceedings of the 34th International Conference on Ocean, Offshore and Arctic (OMAE2015)*. St. John's, Newfoundland, Canada.
- [4] Karlsen, A.T., 2012. On Modeling of a Ship Propulsion System for Control Purposes (Master's thesis, Institutt for teknisk kybernetikk).

# Preparation for replicating empirical study of a selection method for software reliability growth models

Ana Vranković<sup>1,\*</sup>, Tihana Galinac Grbac<sup>2</sup>

<sup>1</sup>University of Rijeka, Faculty of Engineering

E-mail: avrankovic@riteh.hr

<sup>2</sup> University of Rijeka, Faculty of Engineering

E-mail: tihana.galinac@riteh.hr

## 1 Introduction

One of the most expansive and time consuming activity during software development is software testing. With extensive testing, higher software reliability is guaranteed, and with higher reliability, software quality is also improved. Topic on how to improve testing phase and how to predict defects has been highly researched recently. Some of the approaches are methods that estimate remaining defects in software. One of those methods are software reliability growth models(SRGMs) that had been researched for a long period of time[1,2]. SRGMs can be used to help test management when deciding to stop the testing process. This study was based on paper by C. Andersson (2006). In that paper, replication of a study, by Stringfellow and Amschler Andrews (2002) was conducted. In original paper[3] they proposed a method for selecting the appropriate model, described on figure 1. The replication[4] was applied the selection method in an empirical study, conducted in a different development environment than the original study. In their study, they show that the selection method was applicable in an environment that was different from the original one. We performed the empirical study on different data with expanded number of models. The data for this replication study were from Eclipse open-source projects, JDT and PDE.

## 2 Case Study

The study was performed using Matlab software for fitting data and for needed calculations. Software was written using generated cftool code that fits the data to model and returns models parameters. Scripts written in Matlab were used to fit the data into different models.

In this study, we used eight different models, that are described in figure 1, to test our data on. Four concave models and four s-shaped models. Concave models and s-shaped models are classification based on the model curve. In s-shaped models there is an assumption that earlier testing is not as efficient as later testing, on the other hand, concave models assume that the number of failures is steadily decreasing as the testing is progressing. In

\* Corresponding author

table 1. we can see comparison to the original study and the first replicated study.

Tab. 1. Project data in original study (1<sup>st</sup> repl.st.) and this, second replicated study (2<sup>nd</sup> repl.st.)

		Duration ST (weeks)	Failures (ST)
Orig.St.	Release 1	18	231
Orig.St.	Release 2	17	245
Orig.St.	Release 3	13	83
1stRepl.St.	Project 1	22	585
1stRepl.St.	Project 2	27	1330
1stRepl.St.	Project 3	25	3839
Preparation St.	JDT	299	6523
Preparation St.	PDE	384	6822

Principal for selecting the most appropriate model was the same as in original and replicated study, based on fitting the data on each and every model. The reliability growth models were applied on data gathered at 60% of planned testing. Best fit was determined by R-value. Running selection method software for each version of software resulted in at least one model that fits requirements(GOF, stability, convergence, etc.).

Model	Type	Equation $\mu(t)$
Goel-Okumoto	Concave	$a(1 - e^{-bt})$ , $a \geq 0, b > 0$
Delayed S-shaped	S-shaped	$a(1 - (1 + bt)e^{-bt})$ , $a \geq 0, b > 0$
Gompertz	S-shaped	$a \cdot b e^{ct}$ , $a \geq 0, 0 \leq b < 1, 0 < c < 1$
Yamada	Concave	$a(1 - e^{-bc(1 - e^{-dt})})$ , $a \geq 0, bc > 0, d > 0$
Musa-Okumoto	Concave	$a \ln(1 + bt)$ , $a, b > 0$
Inflected S-shaped	S-shaped	$a \frac{1 - e^{-bt}}{1 + ce^{-bt}}$ , $a \geq 0, b > 0, c > 0$
Logistic	S-shaped	$\frac{a}{1 + ce^{-bt}}$ , $a \geq 0, b > 0, c > 0$
Generalized Goel	Concave	$a(1 - e^{-bt^c})$ , $a \geq 0, b > 0, c > 0$

Fig. 1. Used SRGMs

### 3 Conclusion

On the testing data, best fit had Logistic model, both on JDT and PDE project. All s-shaped models gave a better prediction than concave models.

In our further work, our aim is to run selection software on data gathered from industry to see if s-shaped models are also a better fit in a different development environment.

### 4 References

- [1] J. Musa, A. Iannino, K. Okumoto, Software Reliability: Measurement, Prediction, Application, McGraw-Hill, New York, NY, 1987.
- [2] A.L. Goel, K. Okumoto, "Time Dependent Error Detection Model for Software Reliability and Other Performance Measures," IEEE Transaction on Reliability, vol. 28, no. 3, (August 1979), pp. 206 - 211.
- [3] Stringfellow C., Amschler Andrews A, An Empirical Method for Selecting Software Reliability Growth Models. Empirical Softw. Engg. 7(4), 319-343 (2002)
- [4] Andersson C., A replicated empirical study of a selection method for software reliability growth models. Empirical Softw. Engg. 12(2), 161-182 (2007)

# Light distribution for the calibration system in Muon $g - 2$ experiment - precise measurement which could lead to new physics

Vedran Vujnović<sup>1</sup>

<sup>1</sup>Division of Experimental and Applied Physics  
 Department of Physics, University of Rijeka  
 Radmile Matejčić 2, 51000 Rijeka  
 E-mail: [vedran.vujnovic@phy.uniri.hr](mailto:vedran.vujnovic@phy.uniri.hr)

## 1 Introduction

With the discovery of the Higgs boson the last piece of the Standard Model of elementary particles (SM) puzzle was put in place. However, in physics there are still some unresolved mysteries that might have an answer in physics beyond the SM. One of the quantities that could give insight into this physics is the value of muon's anomalous dipole magnetic moment,  $a_\mu$ . Actually, measured quantity is muon's gyromagnetic ratio  $g = 2(1 + a_\mu)$  which is related to anomalous dipole magnetic moment. Gyromagnetic ratio differs from its expected value of 2 because of the quantum fluctuations in the electromagnetic field around the muon. Present value due to the SM theoretically prediction is  $g = 2,0023193043617$ , with uncertainty  $\delta a_\mu^{SM} \cong \pm 49 \cdot 10^{-11}$ [1]. Since theory must be followed by experiment, precision measurements are performed in accelerators and compared with theoretical predictions, to see whether and by how much experiment agrees with theory. During several measurements in the second half of the 20<sup>th</sup> century, maximum achieved experimental accuracy was 7,3 ppm[1] while in the last experiment, which concluded in 2001 at Brookhaven National Laboratory (BNL E821) measurement precision was increased and found discrepancy of 0,54 ppm between the theoretical calculation of  $g$  and its measured value. Found discrepancy was greater than three standard deviation ( $\approx 3,6 \sigma$ ) as shown in Fig.1., but necessary level for claiming a discovery is  $5 \sigma$ , so physicists started to believe that this was not just an error, but the possibility that muon's gyromagnetic ratio is altered by vacuum particles appearing from and disappearing back into the vacuum [2].

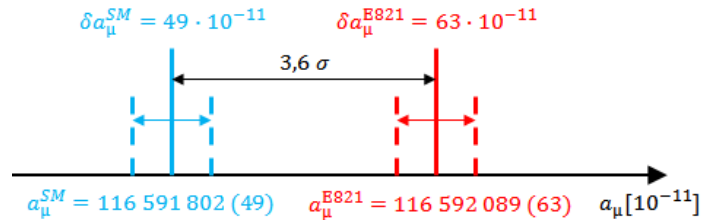


Fig. 1. Discrepancy between theory according to the SM and precise measurement in BNL E821 experiment

## **2 Fermilab Muon $g - 2$ experiment and light distribution for the calibration system**

Fermilab's Muon  $g - 2$  experiment (FNAL E989) goal is to get four-fold better precision compared to BNL E821 experiment i.e. to get overall experimental accuracy of 0,14 ppm. This will allow researchers to peer into the subatomic world to search for undiscovered particles that may be hiding in the vacuum, and hence it will probe fundamental properties of matter and space, and consequently examine completeness of the SM [2, 3].

To achieve higher precision, it is necessary to reduce systematic error of the detector, which will be used to detect positrons produced in a muon decay. Calorimeter is detector's main component for measuring energy and time of arrived positrons, hence the calibration of the calorimeter is required. The calorimeter type and design was already optimized by previous experiments, hence, it was necessary to "deliver" light to the calorimeter in accurate way.

## **3 Measurement results and discussion**

A candidate light distribution system for calibration of the calorimeter was developed and tested. Proper light distribution was obtained using precisely designed mechanical system with laser beam splitters. Its design is based on use of the beam splitters with various reflectivities and fiber splitter for initial distribution. Initial tests were performed with beam splitters with only one reflectivity value due to financial constraints. However, this does not influence its mechanical properties and does not change the conclusion about the feasibility of the system. First assembly and mechanical tests were performed with ordinary glass which was optically characterized before. Preliminary optical tests on output beam matrix (OBM) were performed and after few iterations, a mechanical design was chosen that ensures easy mounting and exchange of the beam splitters as well as accurate beam propagation inside distribution system. Newly developed system is mechanically stable considering external vibration in Storage Ring (main part of FNAL E989 where muon decay occurs) that could occur and cause resonance and consequently failure during calibration process. Using this setup, calculation procedure for theoretical prediction of OBM reflected intensities is developed. Simplicity of the procedure is that we only need two input parameters per polarization state to predict all (54) OBM intensities. Series of optical tests were done with optical grade glasses specially produced for the final assembly. The reflectivity was 1% lower than specified, but in principle, measured discrepancy is within required precision. The results of OBM measurements matched the predicted intensities within 10%. Few values differed by more than 20% but it was attributed to the contamination of the optical elements. Fiber splitter performance was within specifications. The stability over time is better than 1%, and the splitting uniformity is also better than 1% as shown in the Fig. 2. These numbers also show that fiber splitter could be used for the final distribution system where only one laser source could be used for all 54 calibration system inputs.

## 4 Conclusion

Overall the system 1296 channels will provide the required uniformity and spatial stability, while the stability over time could show some long-term effects which were not investigated in this work. This is probably not important since longest calibration run duration is foreseen to take at most 2 hours. However, additionally tests on the long-term stability and its dependency on the number of guided modes should be performed.

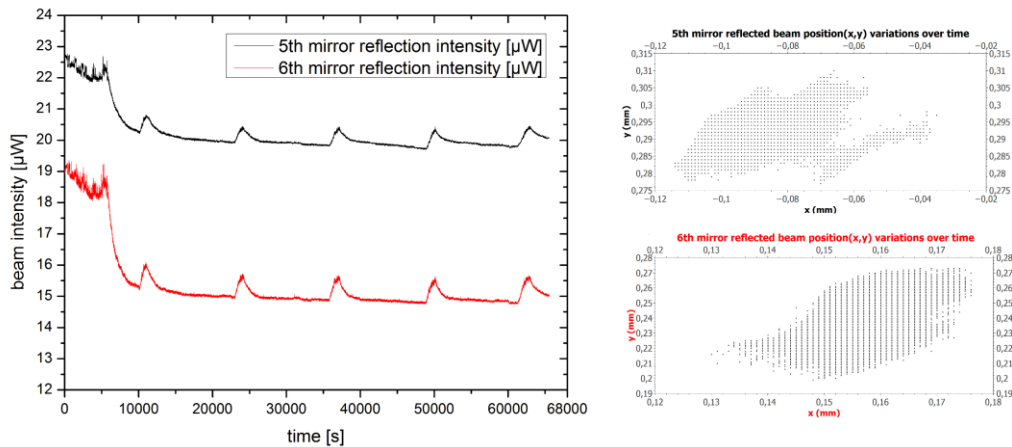


Fig. 2. Reflected beams with longest optical path intensity stability over time and position variation over time

## References

- [1] Gorringe, T.P. and Hertzog., 2015. Precision Muon Physics. *Progress in Particle and Nuclear Physics*, Volume 84, pp.73-123.
- [2] Venanzoni, G., 2014. The New Muon g-2 experiment at Fermilab. *Nuclear and Particle Physics Proceedings*, Volumes 273-275, pp.584-588.
- [3] Anastasi, A. *et al.* 2015. Test of candidate light distributors for the muon (g-2) laser calibration system. *Nuclear Instruments and Methods in Physics Research Section A: Accelerators, Spectrometers, Detectors and Associated Equipment*, Volume 788, pp.43-48.

# Numerical Model of Natural Convection in the Artificial Lake Butoniga

Luka Zaharija<sup>1,\*</sup>, Vanja Travaš<sup>2</sup>

<sup>1</sup>University of Rijeka, Faculty of Civil Engineering  
E-mail: [luka.zaharija@student.uniri.hr](mailto:luka.zaharija@student.uniri.hr)

<sup>2</sup>University of Rijeka, Faculty of Civil Engineering  
E-mail: [vanja.travas@gradri.uniri.hr](mailto:vanja.travas@gradri.uniri.hr)

## 1 Introduction

Butoniga is an artificial lake situated in central Istria, Croatia. Its purpose is twofold: to prevent flooding of the Mirna valley and to secure water supply of cities in Istria. Since Lake Butoniga is used for water supply, it is important to monitor parameters that affect water quality.

Layer of water near the bottom of the lake is the worst in terms of water quality. It is depleted of oxygen and rich in minerals and chemical compounds such as iron, manganese and phosphate. In autumn, with decreasing air temperature, natural convection of water induces a mixing of upper and lower water layers. Since this can negatively affect water quality and accelerate eutrophication processes, an early autumn discharge of water through bottom outlet is performed every year.

Goal of this work is to develop numerical model of lake Butoniga capable of calculating natural and forced convection of water in case of early autumn discharge and its effects on water quality.

## 2 Numerical model

Computer program used to calculate early autumn discharge is OpenFOAM. It consists of multiple solution algorithms called solvers. Users choose solvers based on natural phenomena that they want to model. In this case, *buoyantBoussinesqPimpleFoam* solver is chosen. It utilises Boussinesq approximation to calculate 3D buoyant flow of incompressible fluids. Boussinesq approximation assumes that fluid density and specific heat capacity are constant. Equations that are solved include Navier-Stokes eq., continuity eq., energy eq., and passive scalar transport eq. (in this case manganese is the passive scalar).

OpenFOAM utility *snappyHexMesh* is used to create finite volume structured hexahedral mesh (Fig. 1.). Size of the hexahedrons is 15x15x1 m. Initial and boundary conditions are implemented according to available data.

## 3 Preliminary Results

For the purpose of calibration and validation of numerical model a 2016 early autumn discharge is being modeled. Measurements taken during discharge process are used to

\* Corresponding author

compare computation results with actual values [1]. Measured and calculated values of water temperature and concentration of manganese at designated point in front of the dam at the end of early autumn discharge are presented in Fig. 2.

#### 4 Conclusions and future work

After comparing measured and computed values it is concluded that numerical model is calibrated and validated. Still, since this is a first numerical model of Butoniga of this type, it has a lot of room for improvement (initial and boundary conditions, inclusion of additional physical processes) and it raises a lot of questions that are yet to be answered.

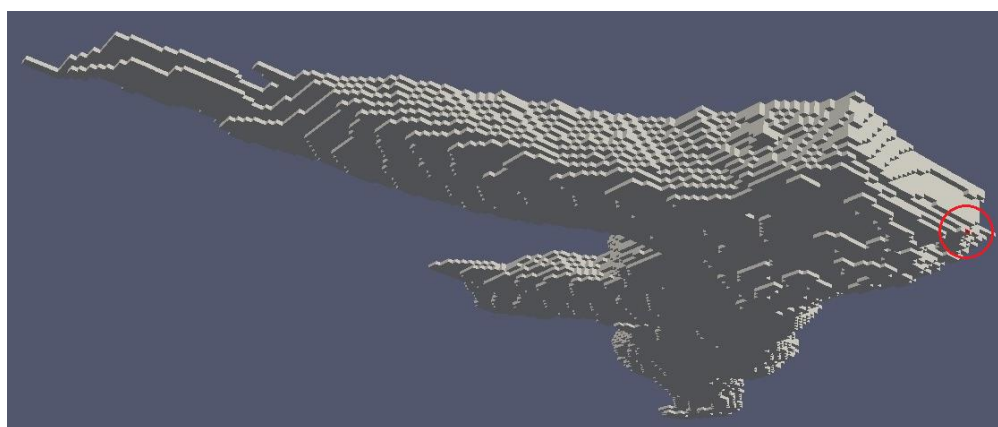


Figure 1: Structured hexahedral mesh with highlighted bottom outlet boundary. Since mesh is very thin, vertical axis dimensions are presented 10 times larger.

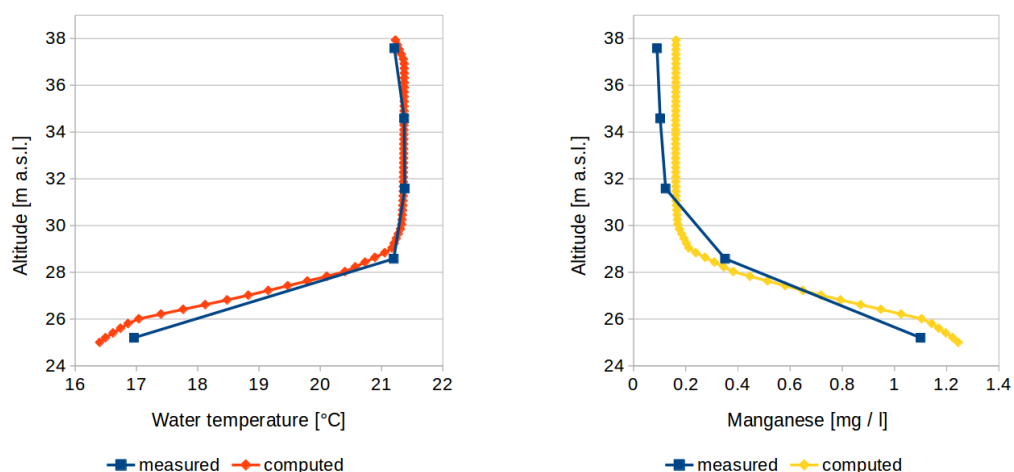


Figure 2: Comparison of measured and calculated values of water temperature and concentration of manganese at different altitudes at the end of early autumn discharge.

#### References

- [1] Mihelčić, N. and Šikoronja, M. and Oštrić, M., 2017. Analiza monitoringa kakvoće vode nakon ranojesenskog ispuštanja 2016. Hrvatske vode.

# Cost-effectiveness of electric vehicles

Filip Žugčić<sup>1</sup>

<sup>1</sup>*Veleučilište u Karlovcu, Trg J.J.Strossmayera 9, 47000 Karlovac, HRVATSKA*  
E-mail: [filip.zugcic@vuka.hr](mailto:filip.zugcic@vuka.hr)

## 1. Introduction

The impact of traffic on modern society is immeasurable. The transport sector is one of the fastest growing industries in the world, as well as in Croatia. The emissions of CO<sub>2</sub> in Croatia by traffic road are about 3 million ton. [1] The transport sector is also the most significant energy consumer with over 30 percent in the total consumption structure, with a tendency to growth in the future. [2] So now is the time to make quality decisions, which will be the foundation of a sustainable transport system development. The development of traffic must be in line with the principles of sustainable development that are already determined at the global or international level. Sustainable traffic does not endanger public health and ecosystems and meets transport demand through rational use of naturally renewable energy sources and non-renewable sources.

Concept of mobility includes electric vehicles, such as personal cars, trucks, buses, but also motorcycles, bicycles that, instead of conventional fuels, are driven exclusively by electric energy. Electric vehicles are constantly growing in popularity, as evidenced by the increasing number of serial models of different manufacturers that can be purchased and already present on our roads.

## 2. Cost-effectiveness of electric vehicles

This part shows scenario where personal cars are divided into several categories, depending on the mileage that passes and on which fuel they are driven.

The first group of vehicles will be marked with “vehicle A”. That includes all personal cars which operate 12,000 km per year, what is the average annual path of personal car. [3] The next group of vehicles are vehicles under the name of “vehicle B”, and in this group cars are with an annual average distance of 6,000 km. The last type of vehicles are vehicles under the name “vehicle C”, they are classified as vehicles used for public transport, e.g. taxi and transiting 100,000 km per year.

Table 1.1. shows input data for different types of vehicles (petrol, diesel, hybrid, electric). Input data includes their average consumption, carbon dioxide emission and fuel prices. [4], [5], [6], [7], [8].

\*the price of kWh electric energy in high tariff.

\*\*the average emission of power generation plants is 300 gCO<sub>2</sub>/kWh (300gCO<sub>2</sub>/kwh · 11,7/100 = 35,1 gCO<sub>2</sub>/km), emission CO<sub>2</sub> of electric vehicle is zero.

Table 1. Input data for different kind of vehicles

Type of vehicle	Fuel prices (kn/l, kn/kWh)		Fuel consumption (l/100km, kWh/100km)	Emission CO <sub>2</sub> (g/km)
Conventional	Petrol	9,39	8	122,7
	Diesel	8,50	6,5	119,2
Hybrid	Petrol	9,39	3,44	88,1
	kWh	0,7131*		
Electric	kWh	0,7131	11,7	35,1**

Table 2. Output data based on input data depending of vehicle type

Fuel costs, CO <sub>2</sub> emission, based on input data											
Type of vehicle		Fuel cost per 100km (kn/100km)	Annual fuel cost (kn/yr.)			Annual CO <sub>2</sub> emission (kgCO <sub>2</sub> /yr.)			Forest area required for absorption CO <sub>2</sub> (m <sup>2</sup> )		
			Vehicle A	Vehicle B	Vehicle C	Vehicle A	Vehicle B	Vehicle C	Vehicle A	Vehicle B	Vehicle C
Conventional	Petrol	75,12	9014,14	4507,2	75120	1472,4	736,2	12270	749	374	6240
	Diesel	55,25	6630	3315	55250	1430,4	715,2	11920	697	348	5810
Hybrid		32,30	3876	1938	32300	1057,2	528,6	8810	318	159	2650
Electric		8,34	1000,8	500,4	8340	421,2	210,6	3510	151	75	1260

Table 2 shows the results of annual fuel consumption and CO<sub>2</sub> emissions for different types of vehicles, which exceed a certain number of kilometers. This table also shows the forest area in square meters required for the absorption of carbon dioxide emitted by different vehicles. [9]

### 3. Conclusion

From the obtained results we can see that the fuel cost of petrol and diesel cars are multiple times bigger than in hybrid and electric cars. Next reason for the viability of investing in electric vehicles is their zero emissions of carbon dioxide into the atmosphere, which is today one of the main tasks of sustainable development and environmental conservation. Today, the prices of electric vehicles are still higher than conventional cars, however, there are a number of countries that provide subsidy for a zero emission-car purchase, while the payoff of such a car is dependent on the mileage that exceeds.

### References

- [1] Gasparovic – Punjenje baterija u električnom automobilu, Diplomski rad
- [2] Grdić Ivana – Javna punionica za električne automobile, Diplomski rad
- [3] [http://www.cvh.hr/media/2431/prosjecno\\_godisnje\\_prijedjeni\\_put\\_povv\\_za\\_2016.pdf](http://www.cvh.hr/media/2431/prosjecno_godisnje_prijedjeni_put_povv_za_2016.pdf)
- [4] <http://cijenegoriva.info/CijeneGoriva.aspx>
- [5] <http://hepi.hep.hr/cjenik>
- [6] <http://www.sciencedirect.com/science/article/pii/S0360128516300442>
- [7] <https://www.toyota.hr/hybrid-innovation/faqs/index.json>
- [8] <https://www.volkswagen.hr/e-up>
- [9] <http://elen.hep.hr/Kalkulator.aspx>